



A non-explicit representation of macropores in the SVS land surface model improves streamflow simulations under frozen soil conditions

Benjamin Bouchard¹, Vincent Vionnet¹, Étienne Gaborit¹, Vincent Fortin¹

¹Meteorological Research Division, Environment and Climate Change Canada, Dorval, H9P 1J3, Canada

5 *Correspondence to:* Benjamin Bouchard (benjamin.bouchard@ec.gc.ca)

Abstract. Soil freezing is a major cold region process that influences hydrological response of northern catchments, in particular during winter rainfall and snowmelt events. Ice within the soil matrix reduces the pore space available for water to infiltrate, while the presence of soil macropores in structured soils maintains rapid water percolation even in frozen conditions. Representing the complex effect of soil freezing on water infiltration in land surface models is a challenging task. This is particularly true for operational models, where physical process integration must balance performance improvements against computational efficiency and complexity. In this study, we propose a conceptual approach to represent the effects of macropores on frozen soil infiltration into the Soil, Vegetation, and Snow (SVS) model used within the operational prediction systems of Environment and Climate Change Canada (ECCC). We assessed the effects of this new configuration (Fr-MP) on streamflow simulations at more than 580 hydrometric stations located in the Great-Lakes and Saint-Lawrence domain over a five-year period. The conceptual representation of macropores improves the Kling-Gupta Efficiency (*KGE*) at 88% of the assessed stations, resulting in an increase in the median *KGE* of 0.28 compared to the configuration without macropores and soil freezing. Detailed analysis of a decomposed hydrograph shows that the Fr-MP configuration increases SVS soil drainage (slow response) and reduces surface runoff and lateral flow (quick response). To ensure that the proposed change is also acceptable in the context of operational numerical weather prediction, an evaluation of its impact on soil freezing depth as well as screen-level temperature and dew point temperature predictions is performed against in-situ observations. These results support the potential operational implementation of the Fr-MP configuration at ECCC for numerical weather and streamflow prediction.

1 Introduction

Roughly half of the land surfaces in the Northern Hemisphere are underlain by permanent or seasonally frozen ground (Zhang et al., 2003). Soil freezing and thawing are major processes in cold regions that are expected to intensify under climate change (Henry, 2008), resulting in significant environmental impacts. Freeze-thaw cycles release greenhouse gases into the atmosphere, amplifying global warming through a positive climate feedback loop (Liu et al., 2024; Wang et al., 2025). Soil freezing and thawing also degrades nutrient cycling by increasing carbon and nitrogen leaching (Campbell et al., 2014; Patel et al., 2018). In terms of hydrology, several floods in cold regions occurred during snowmelt under frozen soil conditions



30 (Barredo, 2007; Neri et al., 2019; Perry, 2000). However, the extent to which soil freezing influences a catchment response to snowmelt and rainfall remains unclear (Ala-Aho et al., 2021; Swenson et al., 2012).

At the soil sample scale, the presence of ground ice prior to snowmelt reduces soil permeability, which limits connectivity between surface and subsurface water, thereby reducing infiltration (Appels et al., 2018; Covino, 2017; Gray et al., 1985). However, this does not necessarily result in a greater runoff at larger scales. According to Wei et al. (2019), the number of
35 freeze-thaw cycles only increases runoff when the initial soil moisture content is low, as demonstrated through a plot-scale experiment in the central US. Shanley and Chalmers (1999) conducted field experiments in northeastern US and observed a correlation between runoff and soil freezing only in a small agricultural plot ($< 1 \text{ km}^2$) but not in a larger catchment ($> 100 \text{ km}^2$). Based on multiple-year experiments in catchments smaller than 20 km^2 located in northern Sweden and Switzerland, Lindström et al. (2002) and Stähli (2017) found that soil freezing has no significant influence on runoff. The discrepancy
40 between infiltration restriction at the laboratory scale and unaffected runoff at plot and catchment scales under frozen soil conditions can be partially explained by soil macropores. Macropores, which originate from biological factors such as earthworms and plant roots (Jarvis, 2007; Six et al., 2004), foster infiltration through preferential flow as they remain air-filled under partially saturated conditions when the soil freezes (Bauer et al., 2025; Demand et al., 2019; Mohammed et al., 2018, 2021; Stähli et al., 1999). This makes complex and challenging the representation of infiltration into frozen ground in numerical
45 models.

Water flow in frozen soil is typically simulated by combining a water transport model, usually the Richards equation, with a heat transfer model (Dall'Amico et al., 2011; Flerchinger and Saxton, 1989; Koren et al., 1999; Zhao and Gray, 1997). The Clapeyron equation is often used to derive a soil freezing curve from a soil moisture curve (Kurylyk and Watanabe, 2013). This is done by assuming that the residual liquid water content decreases with increasing negative temperature in the same
50 way that soil moisture decreases with increasing negative pressure (Miller, 1980). However, this method is computationally intensive because it requires solving coupled nonlinear systems. Simpler models estimate phase change using linear heat conduction algorithms between adjacent soil layers (Hayashi et al., 2007; Mohammed et al., 2013) or include a simplified solution of Stefan's equation (Changwei and Gough, 2013; Krogh et al., 2017; Krogh and Pomeroy, 2021). Still, these methods ignore convective heat exchanges and do not consider the freezing point depression caused by high negative pore pressure
55 (Zhang et al., 2022).

To account for the formation of ice in the porous space and the resulting decrease in soil hydraulic conductivity (Burt and Williams, 1976; Harlan, 1973), numerous models use an empirical impedance factor when ice partially occupies pore space (Ganji et al., 2017; Hansson et al., 2005; Lundin, 1990; Mao et al., 2007; Smirnova et al., 2000; Taylor and Luthin, 1978). In most of these models, flow impedance increases with ice content following a power law function (Jame and Norum, 1980),
60 which strongly limits frozen zone permeability and infiltration capacity (Kurylyk and Watanabe, 2013; Watanabe, 2008). As a result, the impedance factor may lead to an overestimation of surface runoff and erroneous hydrological simulations (Agnihotri et al., 2023). One option for promoting more infiltration into frozen soil is to simulate a high-flow regime that corresponds to the macropore network and a low-flow regime that represents matrix flow (Larsbo et al., 2005; Šimůnek et al.,



2003; Stähli et al., 1996; Weigert and Schmidt, 2005). However, models that use such a dual-domain approach do not explicitly
65 represent the physics of macropore flow because there is still no consensus on how to describe this process in numerical models
(Jarvis et al., 2016). This may partially explain the difficulties encountered when simulating infiltration and runoff partitioning
under frozen soil conditions, particularly at large spatial scales (Ala-Aho et al., 2021; Mohammed et al., 2018).

When developing land surface schemes (LSS) for real-time hydro-meteorological forecasting, one must generally make
tradeoffs on model complexity to achieve improvements in forecast skill while meeting constraints on computing resources
70 cost and timeliness of the forecasts. In this context, Environment and Climate Change Canada (ECCC) adheres to the same
principles as the European Centre for Medium-range Weather Forecasts (ECMWF): only add complexity if there is a route to
successfully initialize and verify that the forecasts are timely, skillful, relevant to users and impactful (Boussetta et al., 2021).
The Soil, Vegetation and Snow (SVS; Alavi et al., 2016; Husain et al., 2016; Leonardini et al., 2020, 2021) LSS developed at
ECCC and designed for operational weather and water forecasting thus falls into a category of intermediate complexity. SVS
75 relies on simple, yet physically-based, parameterizations of surface physical processes, with the capacity to be integrated in
both numerical weather prediction and hydrologic forecasting systems.

SVS simulates vertical flow between soil layers using a single domain approach, assuming that unsaturated Darcian flow is
the only mechanism by which water is conveyed (Soulis et al., 2000, Alavi et al., 2016). The soil freezing scheme from the
Versatile Soil Budget Model (VSBM; Mohammed et al., 2013) based on the simple heat-conduction algorithm from Hayashi
80 et al. (2007) has recently been implemented into SVS to represent phase changes in the soil column (Amani et al., 2025). The
soil freezing module of SVS accounts for the reduction of the porous space due to ice and invokes the same impedance factor
as computed in the CLASS LSS to limit infiltration when soil ice is simulated (Ganji et al., 2017). However, at the time of
writing, soil freezing and thawing in SVS is not yet activated in ECCC's operational forecasting systems as it generally leads
to unrealistic predictions of spring freshets, as mentioned in Gaborit et al. (2025).

85 The main objective of this work is to improve streamflow prediction under frozen soil conditions by integrating a simple, non-
explicit representation of soil macropores into the SVS LSS. The hydrological impact of this proposed configuration is assessed
against SVS configurations without soil freezing, and with soil freezing but without macropores, through a multi-year
evaluation over a large domain that encompasses watersheds in the eastern US and Canada. Improving frozen soil infiltration
in SVS would enable the activation of soil freezing and thawing processes within the operational framework of ECCC.

90 **2 Material and methods**

2.1 Code description

2.1.1 Default SVS configuration without soil freezing

ECCC uses the GEM-Hydro hydrometeorological modelling platform (Gaborit et al., 2017; Vionnet et al., 2020) within the
National Surface and River Prediction System (NSRPS). The NSRPS aims to provide the most accurate real-time surface and



95 hydrologic analyses and forecasts for Canadian and Canada/US transboundary watersheds while maintaining the quality of
surface weather forecasts (Durnford et al., 2021). GEM-Hydro combines two main components: GEM-Surf, which simulates
processes at the surface (Bernier et al., 2011) and Watroute for river routing (Kouwen, 2010).
GEM-surf divides each continental surface grid cell into multiple tiles and relies on SVS to represent vegetated areas and bare
ground within each grid cell (Alavi et al., 2016; Husain et al., 2016; Leonardini et al., 2021). In SVS, the energy budget
100 between the surface and the atmosphere is computed independently for four types of land surfaces: snow-free bare ground;
snow-free low and high vegetation; snow over bare ground and low vegetation; and snow below high vegetation. The evolution
of snow, vegetation, and bare ground surface temperatures is estimated using respective force-restore schemes (Husain et al.,
2016; Leonardini et al., 2021). SVS also simulates soil hydrology as a single column of multiple layers solving Richards
equations for unsaturated Darcian flow (Alavi et al., 2016).

105 Precipitation and snowmelt that reach the ground surface can exit the grid cell as surface runoff or infiltrate into the upper soil
layer. Surface runoff occurs when the rate at which liquid water accumulates over the surface exceeds the vertical hydraulic
conductivity ($K_{sat,v}$) of the upper soil layer, or when a portion of this layer becomes saturated which is dependent on the pore
size distribution and bulk saturation of the first layer at the subgrid-scale (Alavi et al., 2016). Water that infiltrates into the soil
column can be conveyed to the layers below using a finite difference solution of the Richards equation, or it can exit the column
110 as lateral flow (Soulis et al., 2000). Lateral flow is calculated based on drainage density and tile slope. It is also influenced by
a depth-dependent anisotropy factor that increases horizontal hydraulic conductivity ($K_{sat,h}$) and facilitates lateral flow for
layers near the surface (Alavi et al., 2016). Lateral flow also occurs when there is insufficient space in the underlying layer to
receive the downward water flux, that is, the excess water is removed as lateral flow. Ultimately, water that reaches the bottom
of the soil column leaves the column as soil drainage when the field capacity of the lowermost layer is exceeded. Within GEM-
115 Surf, SVS includes an optional, non-explicit representation of the effects of tile drains and ploughing in agricultural areas
(Gaborit et al., 2025). For simulating the effect of tile drains, a multiplicative coefficient, m_h , is applied to the $K_{sat,h}$ of the fifth
soil layer (between 40 and 100 cm deep), which is further weighted by the fraction of agricultural cover in the land tile of the
grid-cell. This results in an increase in lateral flow. Similarly, the effect of ploughing is modeled by applying a multiplicative
factor, m_v , to the vertical hydraulic conductivity $K_{sat,v}$ of the first three soil layers (between the surface and 20 cm deep), which
120 increases vertical water transport near the surface. In our study, the multiplicative factors for the effect of tile drains and
ploughing were set to 500 for m_h and 10 for m_v . These values are based on the calibration work performed by Gaborit et al.
(2025) and allow to promote greater lateral flow in agricultural catchments. Figure 1a provides a conceptual overview of the
soil water fluxes in the default version of SVS without soil freezing. An explicit description of it can also be found in Alavi et
al. (2016).

125 Watroute (Kouwen, 2010) is a gridded routing scheme that conveys water through a network of rivers and lakes to simulate
streamflow and water levels. The version used at ECCC can explicitly represent diversions, lakes and reservoirs, using the
dynamically zoned target release model for the latter (Gaborit et al., 2022; Yassin et al., 2019). Surface runoff and lateral flow
from GEM-Surf contribute directly to the surface network in Watroute. In contrast, soil drainage is added to the lower zone

storage of Watroute, which is a conceptual reservoir used to represent aquifers and simulate baseflow, which is then also
130 provided to the surface network in Watroute.

2.1.2 Soil freezing module

The version of SVS used in GEM-Surf includes an optional representation of soil freeze/thaw processes which is described in
Amani et al. (2025). The following section provides a summary of the soil freezing module in SVS, emphasizing new additions
to the module.

135 The soil freezing module relies on a simple heat-conduction algorithm (Hayashi et al., 2007) described in the VSBM model
(Mohammed et al., 2013). This approach estimates the temperature and phase changes for each soil layer and uses the upper
boundary condition provided by force-restore schemes. Compared to the iterative solutions of coupled nonlinear equations,
this approach is less computationally intensive and suits the level of complexity of the force-restore schemes used for the
surface energy balance in SVS.

140 The heat conduction algorithm in SVS assumes that the change in net heat flux for any given layer corresponds to the change
in stored latent and sensible heat and is calculated sequentially from top to bottom within the soil column. This simple approach
ignores the freezing-point depression and water in soil pores is assumed to freeze at $T_{ref} = 273.15$ K (Kurylyk and Watanabe,
2013). However, liquid water can remain at sub-zero temperatures and coexist with ice. When the soil layer temperature is not
equal to T_{ref} (i.e. when the layer is completely thawed or frozen), the change in net heat flux converts into sensible heat until
145 the soil layer temperature reaches T_{ref} . When the soil layer temperature equals T_{ref} , the change in net heat flux is first used for
melting or freezing all available water above the residual unfrozen water content, converting any residual energy into sensible
heat.

The residual unfrozen water content depends on soil texture and saturated water content based on Niu and Yang (2006). Their
model allows to derive the maximum unfrozen water content as a function of soil texture and temperature. However, since
150 SVS assumes that phase change only occurs at 273.15 K, a unique residual unfrozen water content is associated to any given
soil texture, regardless of soil temperature under frozen conditions. It corresponds to the average of the values obtained from
Eq. (3) of Niu and Yang (2006) for different soil temperatures:

$$W_{res} = \frac{W_{sat} \sum_{i=1}^{n=5} \left[\frac{10^3 L_f (T_i - T_{ref})}{g T_i \psi_{sat}} \right]^{-1/b}}{n} \quad (1)$$

where the temperature, T_i , increases from 263.15 to 271.15 K by five increments of 2 K and L_f and g are the latent heat of
155 fusion (334 J kg^{-1}) and the gravitational constant (9.81 m s^{-2}), respectively. The saturated water content, W_{sat} (unitless), the
saturated soil matric potential, ψ_{sat} (mm), and the slope of the water retention curve from Clapp and Hornberger (1978), b
(unitless), are all soil texture-dependent parameters:

$$W_{sat} = -0.00126 X_{sand} + 0.489 \quad (2)$$

$$\psi_{sat} = \frac{10^{(-0.0131 X_{sand} + 1.88)}}{100} \quad (3)$$



160 $b = 0.137X_{clay} + 3.501$ (4)

with X_{sand} and X_{clay} being the sand and clay percentages (between 0 and 100) of any soil layer, respectively.

For phase change computation, we apply an efficiency factor based on the soil water content of each layer similar to that used in the ISBA model (Boone et al., 2000):

$$\chi_{fr} = (W - W_{res})/W_{sat} \quad (5a)$$

165 $\chi_{th} = I/(W_{sat} - W_{res})$ (5b)

where χ_{fr} and χ_{th} are respectively the efficiency factors for freezing and thawing (unitless), W is the soil moisture and I is the volumetric ice fraction, both unitless. This approach implies that a given soil layer with high soil moisture (ice) content freezes (thaws) more rapidly than when it contains less liquid water (ice)(Pitman et al., 1991). The minimal value that χ_{fr} and χ_{th} can take was set to 0.6.

170 The lower boundary condition for temperature is set at a depth of 2.5 times the total thickness of the soil column. For a typical SVS soil configuration of a 3 m depth, this corresponds to a depth of 7.5 m. This approach aims to minimize the error in both soil water and energy budgets (Decharme et al., 2013). The upper boundary condition is the sum of the heat fluxes from each of the four surface energy budgets (see Sect. 2.1.1), weighted by their respective fractions. For bare ground, the heat flux varies according to the difference between the skin temperature from the soil force-restore scheme and the temperature of the surface
175 soil layer. Recent improvements in the soil freezing scheme of SVS make that the release and absorption of latent heat due to soil freezing and thawing now impact the evolution of the temperature variables of the bare ground in the force-restore scheme as follows:

$$\Delta T_{grnd,j} = \chi_j L_f C_g \Delta W_{LH} \quad (6)$$

where $\Delta T_{grnd,j}$ is the gain (loss) of surface or deep bare ground temperature (in K) in the force-restore scheme associated to the
180 release (absorption) of mass from the latent heat flux (ΔW_{LH} ; in kg m^{-2}). χ_j corresponds to the efficiency factor for freezing in the case of latent heat release ($\Delta T_{grnd,j}$ positive) and for melting, inversely. C_g is the soil thermal coefficient for the force-restore scheme (in $\text{K m}^{-2} \text{J}^{-1}$) based on soil porosity and texture, and on water and ice content for the topmost soil layer. The latent heat flux from the upper 5 cm is considered for $\Delta T_{grnd,surf}$ while the latent heat flux of soil layers between 5 and 100 cm deep is used for $\Delta T_{grnd,deep}$.

185 For snow-free vegetation (low and high), a constant skin conductivity of $10 \text{ W K}^{-1} \text{ m}^{-2}$ is applied to the difference between the vegetation skin temperature and the temperature of the upper soil layer for estimating the heat flux (Boussetta et al., 2021). For bare ground, a constant skin conductivity of $15 \text{ W K}^{-1} \text{ m}^{-2}$ is used. The heat flux between the ground and the snowpack depends on the snow thermal conductivity and on the difference between the deep snow temperature from the force-restore scheme and the surface layer temperature, if the snow depth is greater than the thermal damping depth. Otherwise, the skin
190 snow temperature is used instead. Equations used for the snow thermal conductivity, and the thermal damping depth are presented in Leonardini et al. (2021). The fraction of the tile covered by snow is estimated using the configuration from Niu and Yang (2007).



The soil freezing module directly impacts soil hydrology. First, available pore space decreases as the ice fraction increases, reducing the available space for liquid water (Zhao and Gray, 1997):

$$195 \quad W_{sat,fr} = W_{sat} - I \quad (7)$$

where $W_{sat,fr}$ is the saturated water content (unitless) adjusted for the presence of soil ice.

Second, the presence of ground ice decreases the $K_{sat,v}$ through an impedance factor, described as follows (Ganji et al., 2017):

$$K_{sat,v,fr} = \left[1 - \min\left(1.0, \frac{I}{W_{sat}}\right)\right]^2 K_{sat,v} \quad (8)$$

where $K_{sat,v,fr}$ (m s^{-1}) is the hydraulic conductivity of the soil layer when it is partially frozen.

200 Overall, simulating soil freezing in SVS has the effect of increasing surface runoff and lateral flow in favor of soil drainage, as shown in conceptual Fig. 1b.

2.1.3 Configuration of macropores

To promote infiltration under frozen soil conditions, we implemented a new option in SVS that mimics the behavior of macropores based on liquid water content. The algorithm verifies if the liquid water content of each soil layer at any given
205 timestep exceeds the macropore activation threshold (W_{MP} , unitless):

$$W_{MP} = \alpha_{MP} W_{sat,fr} \quad (9)$$

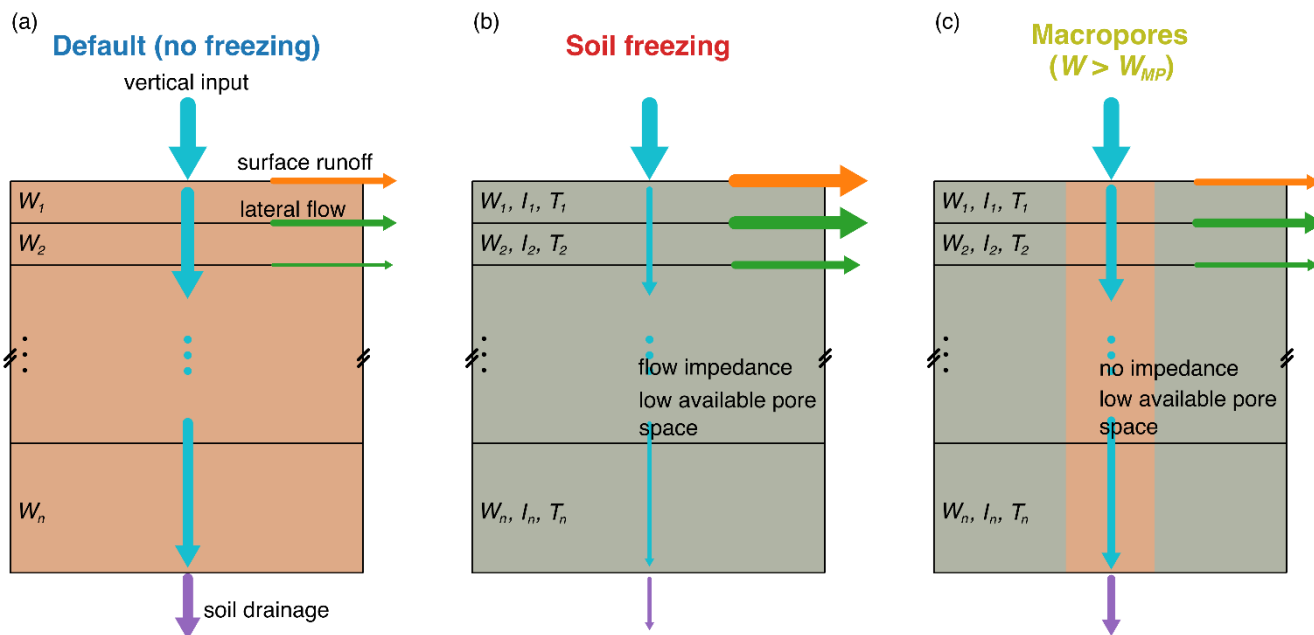
where α_{MP} is a calibrated parameter between 0 and 1 representing the fraction of saturated water content to be considered for activating macropores. We chose a dependency on soil moisture for activating the effect of macropores on infiltration since the routine for water diffusion in unsaturated porous media from Soulis et al. (2000) used in SVS resolves Richards equation
210 based on the water content (Alavi et al., 2016). Although macropore flow is activated based on a soil matric potential threshold in most models (Šimůnek et al., 2003), it has been shown experimentally in many studies that non-equilibrium flow in the soil is more likely when the soil conditions are moist rather than dry (Alaoui, 2015; Bauer et al., 2025; Beven and Germann, 2013; Jarvis, 2007).

In the configuration proposed here, when W exceeds W_{MP} , the effect of ice on flow impedance is not considered such that
215 $K_{sat,v,fr} = K_{sat,v}$. In other words, activating macropores increases the vertical hydraulic conductivity of frozen soils as if it was unfrozen. Thus, when the soil is completely unfrozen and $W > W_{MP}$, there is no effect on the soil hydraulic conductivity. This simple and non-explicit approach aims to increase infiltration into frozen soils while remaining simple to implement operationally compared to other models relying on dual-domain approaches (Larsbo et al., 2005; Ross and Smettem, 2000; Šimůnek et al., 2003; Stähli et al., 1996).

220 To further increase infiltration, we implemented an additional feature to the new macropore representation, such that surface runoff occurs only when the vertical water input rate exceeds the infiltration rate. It implies that mechanisms for generating runoff at the subgrid-scale (i.e. seepage saturation at the surface), as presented in Sect. 2.1.1, do not lead to surface runoff anymore. This new feature, which is always activated, influences runoff-infiltration partitioning when the surface soil layer



approaches saturation, which is mainly the case in presence of soil ice. A conceptual illustration of flow in SVS under the new
 225 macropore representation is shown in Fig. 1c.



230 **Figure 1: Conceptual scheme of the soil water balance in SVS (evapotranspiration is not shown here) for (a) the default configuration without soil freezing, (b) the soil freezing configuration and (c) the configuration of soil freezing with the macropores. W denotes the water content of layer i while I and T denote the ice fraction and the temperature of layer i , respectively, on (b) and (c). Vertical downward water flux through the soil column is shown by blue arrows while orange, green and purple arrows correspond to surface runoff, lateral flow and soil drainage, respectively. The relative size of the arrows represents the relative magnitude of the fluxes in each configuration.**

2.2 Modeling setup

The study area covers the Great-Lakes and Saint-Lawrence (GLSL) domain, which includes the five Great-Lakes watersheds
 235 (Lake Superior, Lake Michigan, Lake Huron, Lake Erie, and Lake Ontario), the Ottawa River Basin (which occupies provinces of Ontario and Québec), and the Saint-Lawrence Valley, including the Saguenay Lac-Saint-Jean watershed in the northeast of the domain (Fig. 2). The northern half of the domain is primarily forested, with a transition from deciduous to coniferous forests from south to north. Agricultural areas dominate the region between Lake Erie and Lake Huron, as well as the southwest of Lake Erie and the shores of the Saint-Lawrence Valley. The GLSL domain also includes urban areas like the Greater Toronto
 240 Area, the Montréal metropolitan area, and the U.S. cities of Chicago, Detroit, Cleveland, and Buffalo, among others. The terrain is relatively flat in most of the Great-Lakes watersheds but becomes hillier in the northeast of the domain, which also includes part of the Appalachian mountains in the Lake Champlain watershed. Note the existence of a large, confined aquifer in southern Michigan (between Lake Michigan and Lake Huron; Lampe, 2009) and the presence of numerous wetlands in the north of Lake Michigan and in southern Ontario (Penfound and Vaz, 2022). These have an influence on streamflow regime
 245 but are not represented explicitly in GEM-Hydro (Gaborit et al., 2025).

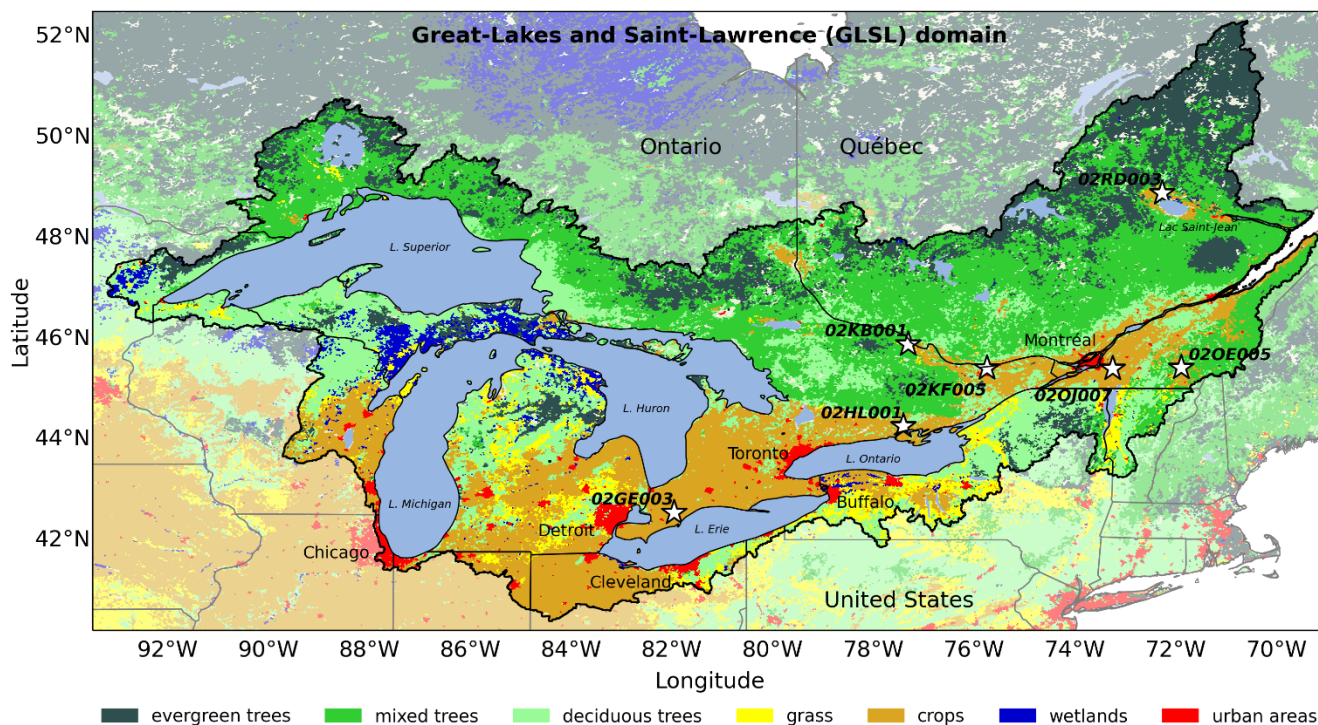


Figure 2: Map of the dominant vegetation class for each grid cell within the Great-Lakes and Saint-Lawrence (GLSL) domain. The location of the hydrometric stations used for the hydrograph analysis is identified by a white star (see Sect. 3.4).

For the evaluation, we considered three open-loop experiments with GEM-Hydro: a first experiment in which the soil freezing module of SVS is not activated (noFr), a second experiment in which the soil freezing module is activated, but the macropores are disabled (Fr), and a third experiment in which the macropores are activated over the soil freezing module (Fr-MP). In all three experiments, we use the geophysical fields described by Gaborit et al (2025) in their final GEM-Hydro setup and we set the soil column as seven soil layers extending down to three meters with increasing thickness.

We ran GEM-Surf and Watroute at spatial resolutions of 2.5 km and 1 km, respectively. GEM-Hydro was forced hourly with the version 3.1 of the Canadian Surface Reanalysis (CaSRv3.1, see Gasset et al., 2025). CaSRv3.1 relies on a 10-km configuration of the GEM atmospheric model (McTaggart-Cowan et al., 2019) which is initialized every 12 hours from the ERA5 atmospheric reanalysis (Hersbach et al., 2020) and is coupled with the Canadian Land Data Assimilation System (CaLDAS, Carrera et al., 2015) and the Canadian Precipitation Analysis (CaPA; Fortin et al., 2015), which uses surface observations and optimal interpolation to produce gridded precipitation reanalysis at 24-hour. The main improvements of CaSRv3.1 compared to the previous version (v2.1; Gasset et al., 2021) are the correction of a cold bias in air temperature in the spring as well as the use of ERA5 instead of ERA-Interim for initial conditions. Precipitation phase was partitioned between liquid and solid based on the near-surface wet-bulb temperature (Wang et al., 2019).



We ran each GEM-Hydro experiment from 1 September 2015 to 31 August 2021, with the first year of simulation (until 31 August 2016) used as a spinup year. Therefore, the evaluation period lasts 5 complete years from 2016 to 2021. We selected
265 this period as it covers years of various hydrometeorological conditions in eastern North America. For instance, the water level of several of the Great Lakes reached new historical records in 2017 and 2019 (Gronewold et al., 2021). This, combined with snowmelt and heavy rainfall in spring, contributed to major flooding in several municipalities of Southern Québec (Jean et al., 2024). In contrast, the year 2020-2021 was exceptionally warm and dry in eastern Canada leading to low-flow conditions in spring (Bouchard et al., 2024; NOAA, 2021).

270 Note that at the time of writing, a version 3.2 of CaSR that includes a bug fix has been released. However, version 3.2 of CaSR is identical to version 3.1 for our period of simulation and has no impact on surface simulations.

2.3 Calibration of the macropore flow

The integration of the macropores implies the addition of α_{MP} , a new parameter indicating the fraction of soil moisture at saturation at which the macropores are activated. We calibrated α_{MP} by running open-loop simulations with GEM-Hydro and
275 activating the macropores using values of α_{MP} starting from 0.5 to 0.99 by increments of 0.05 over the GLSL domain. We used the CaSRv3.1 reanalysis to force the model from 1 September 2015 to 31 August 2018 with the first complete year used as a spinup. The rest of the setup is configured the same as that mentioned in Sect. 2.2.

We set the upper boundary for the sensitivity analysis to $\alpha_{MP} = 0.99$ given that macropore flow is more likely to occur under near saturation conditions (Beven and Germann, 2013; Jarvis, 2007). The lower boundary of the sensitivity analysis is based
280 on irrigation experiments and one-dimensional water flow modeling with MACRO (Stenemo and Jarvis, 2010) performed by Alaoui (2015) who suggested that the soil moisture threshold beyond which macropore flow is initiated is approximately half of the saturated water content.

2.4 Evaluation data and metrics

2.4.1 Simulated streamflow

285 The GLSL domain encompasses a network of hydrometric stations distributed across U.S. and Canada. The U.S. daily streamflow observations were retrieved from the USGS database (https://waterdata.usgs.gov/nwis/dv?referred_module=sw&search_criteria=site_tp_cd&submitted_form=introduction) while the Canadian daily streamflow observations come from the HYDAT database (<https://www.canada.ca/en/environment-climate-change/services/water-overview/quantity/monitoring/survey/data-products-services/national-archive-hydat.html>).

290 During the evaluation period (2016-2021), streamflow observations were available for 581 stations across the domain.

We evaluated the streamflow simulation performances of the three experiments based on three metrics: the relative percent bias (*PBIAS*), the Nash Sutcliffe Efficiency (*NSE*; Nash and Sutcliffe, 1970) and the Kling Gupta efficiency (*KGE*; Kling et al., 2012).



The *PBIAS* (%) can be expressed as follows:

$$295 \quad PBIAS = 100 \frac{\sum_{i=1}^N (S_i - O_i)}{\sum_{i=1}^N O_i} \quad (10)$$

where N is the total number of observation-simulation pairs, and S_i and O_i are the simulated and observed daily streamflow for day i ($\text{m}^3 \text{s}^{-1}$), respectively. According to Eq. 9, a positive (negative) *PBIAS* denotes that the model overestimates (underestimates) the observed streamflow.

The *NSE* $[-\infty, 1]$ is a normalized variant of the Mean Squared Error and can be written as follows:

$$300 \quad NSE = 1 - \frac{\sum_{i=1}^N (S_i - O_i)^2}{\sum_{i=1}^N (O_i - \bar{O})^2} \quad (11)$$

where \bar{O} is the mean of the observed daily streamflow. A *NSE* of 1 means that the simulations perfectly agree with the observations.

Finally, the *KGE* $[-\infty, 1]$ is one minus the Euclidean distance computed between the bias, the variability and the correlation based on their cartesian coordinates:

$$305 \quad KGE = 1 - \sqrt{(r - 1)^2 + \left(\frac{\bar{S}}{\bar{O}} - 1\right)^2 + \left(\frac{CV_S}{CV_O} - 1\right)^2} \quad (12)$$

where r is the Pearson correlation coefficient, \bar{S} is the mean of the simulated streamflow ($\text{m}^3 \text{s}^{-1}$), CV_S and CV_O are coefficients of variability of the simulated and observed daily streamflow ($\text{m}^3 \text{s}^{-1}$), respectively. A *KGE* of 1 implies that the first and second statistical moments (the mean and the variance) of the observed and simulated streamflow are the same and that both samples are perfectly correlated.

310 When comparing two or more experiments for a given station, we decided to exclude the station from the analysis if the *NSE* or *KGE* of at least one experiment was lower than 0 and -0.41 , respectively. Scores below these thresholds indicate that the mean of the observations is a better predictor of streamflow than the model (Knoben et al., 2019). We use this approach to ensure that our analysis includes only stations for which the reference experiment (noFr or Fr) yields reasonable results or is improved by the addition of soil freezing with or without macropores.

315 2.4.2 Near-surface meteorological variables and freezing depth

The surface component of GEM-Hydro has been developed to be used for offline applications such as the NSRPS as well as coupled applications in the context of Numerical Weather Prediction systems. For this reason, we evaluate the impact of soil freezing and the activation of macropores on near-surface meteorological variables: 2 m air temperature (TT , in $^{\circ}\text{C}$) and the 2 m dew point temperature (TD ; in $^{\circ}\text{C}$). The two variables are obtained from GEM-Hydro by interpolating between values at the surface and values of the height of the CaSRv3.1 forcing level using vertical profiles derived from Monin-Obukhov stability theory. The evaluation was performed by comparing hourly model simulations to *in-situ* observations from METAR, SYNOP and SWOB observation networks over the whole domain. In total, this corresponds to 667 stations for the 2016-2021 evaluation period. We evaluated each experiment by computing the mean bias (*BIAS*), the root mean squared error (*RMSE*) and the



standard deviation of the error (*STD*). Then, we computed the difference in performance between the Fr and noFr experiments
325 and between the Fr-MP and the noFr experiments.

The *BIAS*, the *RMSE* and the *STD* are computed using Eq. 13 to 15:

$$BIAS = \frac{1}{N} \sum_{i=1}^N (S_i - O_i) \quad (13)$$

$$RMSE = \sqrt{\frac{1}{N} \sum_{i=1}^N (S_i - O_i)^2} \quad (14)$$

$$STD = \sqrt{\frac{1}{N} \sum_{i=1}^N (X_i - \bar{X})^2} \quad (15)$$

330 where S_i and O_i are the simulated and observed values for either *TT* or *TD*. X_i is the difference between the modeled and
observed value ($S_i - O_i$) for time-step i and \bar{X} is the average of the differences of all observation-simulation pairs.

The difference in *BIAS*, *RMSE* and *STD* between experiments is expressed as shown by Eq. 16 to 18:

$$\Delta BIAS = |BIAS_{noFr}| - |BIAS_{exp}| \quad (16)$$

$$\Delta RMSE = RMSE_{noFr} - RMSE_{exp} \quad (17)$$

335 $\Delta STD = STD_{noFr} - STD_{exp} \quad (18)$

where $\Delta BIAS$, $\Delta RMSE$ and ΔSTD are the differences in *BIAS*, *RMSE* and *STD* in °C while the index *exp* denotes either Fr or
Fr-MP experiments. The *BIAS*, the *RMSE* and the *STD* are in °C.

Finally, we evaluated the capacity of the Fr and Fr-MP experiments to accurately simulate the freezing depth. We define the
freezing depth (*FD*) as the depth of the upper boundary of the last layer in which the ice fraction is greater than zero, plus the
340 fraction of the porous space occupied by ice in that layer, multiplied by its thickness:

$$FD = z + \frac{l}{(w_{sat} - w_{res})} \Delta d \quad (19)$$

where z and Δd (both in m) are, respectively, the depth of the upper boundary and the thickness of the deepest frozen soil layer.
The modeled *FD* is then compared to observations retrieved from the North Central River Forecast Center database
(https://www.weather.gov/ncrfc/LMI_ncrfc_forecast_products), which includes manual freezing depth measurements taken at
345 103 locations in the central U.S. from 2016 to 2021. The bi-monthly mean of the modeled and observed *FD* at all locations
was computed to evaluate the model bias, *RMSE* and standard deviation of the error (Eq. 13, 14 and 15).

3 Results

3.1 Hydrologic impact of soil freezing without macropores

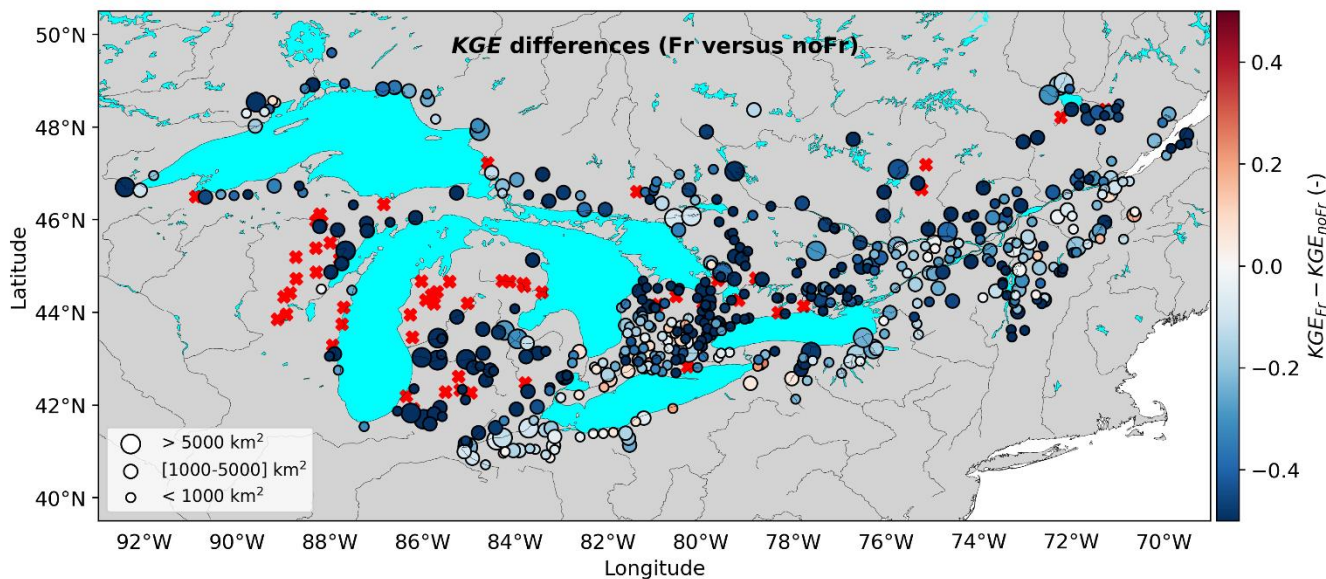
Figure 3 illustrates the differences in *KGE* between the soil freezing (Fr) and the no freezing (noFr) experiments over the
350 Great-Lakes and Saint-Lawrence domain from 2016 to 2021. As Fig. 3 shows, incorporating soil freezing into the model
without a mechanism to promote infiltration degrades streamflow simulations at 92% of the stations, spread all over the domain
($\Delta KGE = -0.44$). This degradation of *KGE* is explained by the degradation of the *NSE* (not shown). This occurs because the



model tends to overestimate streamflow peaks in winter and spring when ground ice is simulated and infiltration is highly restricted.

355 The *KGE* is degraded by more than 0.5 for 172 stations (33%). These stations are primarily concentrated in Michigan, where the perched aquifer is present, as well as along the Niagara Escarpment between Lake Ontario and Lake Huron, where the exchange of surface and groundwater is enhanced, contributing to a larger base flow. The model does not account for these phenomena, which could further degrade its performance when combined with soil freezing configuration.

Most of the stations where the experiment results in a better *KGE* than the noFr experiment (warm-colored dots) are located
360 in agricultural and urban areas, where reactive runoff is favored by tile drains and surface imperviousness, respectively. It is possible that soil freezing compensates for the fact the model does not fully represent the effect of tile drain and urban areas in some catchments, as shown by the use of larger values for m_h and m_v .



365 **Figure 3:** Map of the *KGE* differences between the soil freezing (Fr) experiment and the experiment without soil freezing (noFr) over the Great-Lakes and Saint-Lawrence domain for the 2016-2021 period. Degradations of the *KGE* with the Fr experiment (negative *KGE* differences) are represented by cold-colored dots. Red crosses show stations excluded from the comparison (see Sect. 2.4.1).

3.2 Optimization of α_{MP}

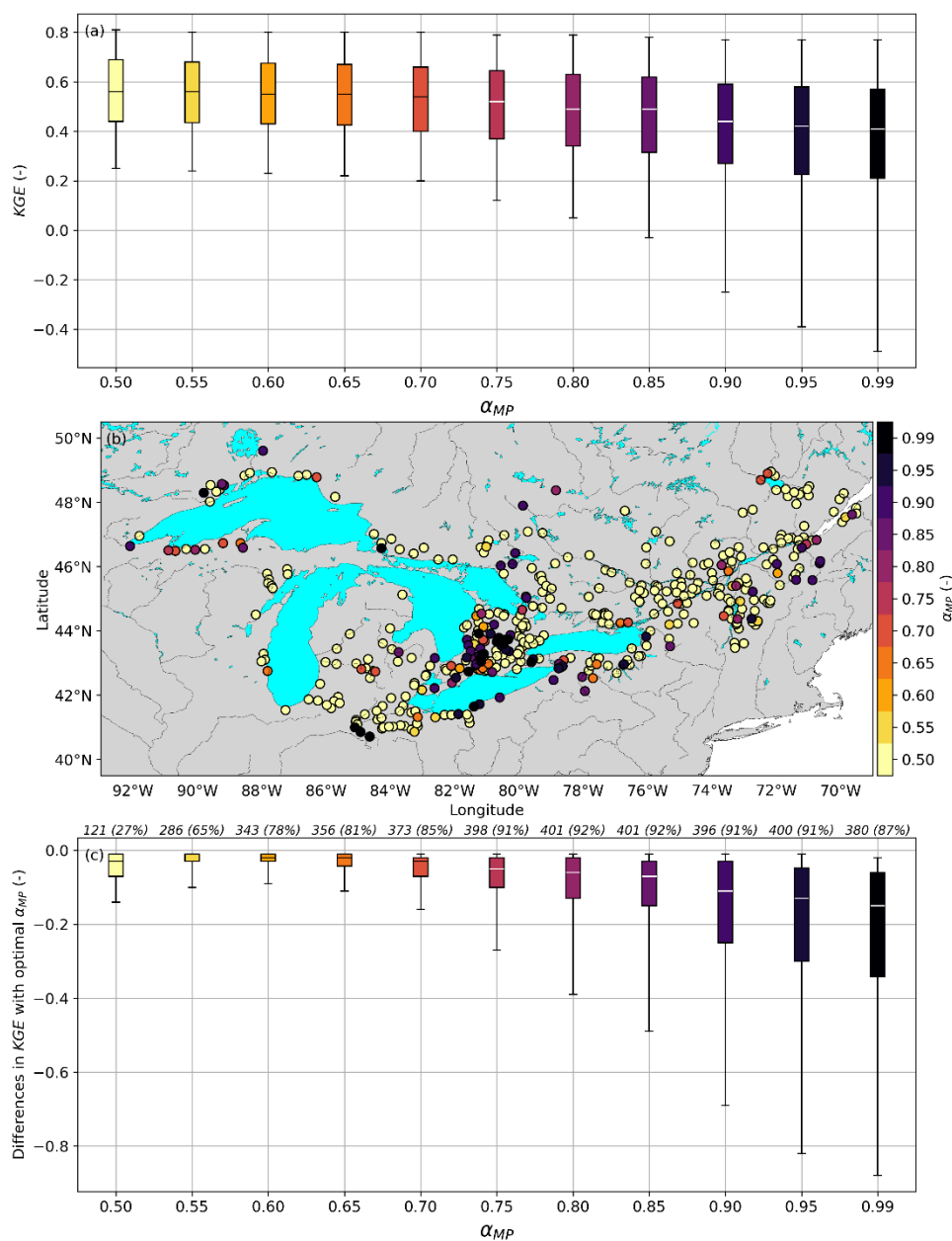
Hydrologic simulations of the soil freezing and macropores configuration (Fr-MP), using incremental values of α_{MP} starting from 0.5, show that the *KGE* is the highest with the lowest α_{MP} values (Fig. 4a). The Fr-MP performance is quite stable when
370 α_{MP} is 0.7 or lower, with a median *KGE* greater than 0.5, and the fifth and ninety-fifth percentiles greater than 0.2 and 0.8, respectively. However, the performance decreases significantly for simulations with larger α_{MP} values. This suggests that the model performs better when a macropore configuration is included over soil freezing because it favors infiltration. Consequently, the lowest *KGE* is obtained in the experiment with the most restrictive infiltration conditions ($\alpha_{MP} = 0.99$). Conceptually, this experiment is similar to the soil freezing configuration without macropores (Fr). This sensitivity analysis



375 demonstrates that adding a simple representation of macropores in SVS improves the *KGE* on the GLSL domain regardless of the value of α_{MP} .

For most stations, a value of α_{MP} of 0.5 leads to a better or equivalent *KGE* than larger values of α_{MP} . These values are uniformly distributed across the domain, as shown by the widely spread yellow dots in Fig. 4b. However, there are a few areas where larger values of α_{MP} perform better. One such area is the center of the domain, between Lakes Huron, Erie, and Ontario, 380 where a small group of nearby stations perform better with an α_{MP} value of 0.99. These stations are all located at the outlet of highly agricultural catchments (see Fig. 2), where a reactive runoff response is favored by the combined effects of tile drains and frozen ground. Note that for several stations, more than one value of α_{MP} results in the best configuration when considering two decimal digits for the *KGE* criterion. In that case, we chose to show the lowest α_{MP} on Fig. 4b.

Figure 4c shows the boxplots of the *KGE* differences between experiments using each α_{MP} value and the experiment with the 385 best *KGE*. We see that a α_{MP} of 0.55 results in the highest median and first quartile compared to the other experiments. Therefore, this experiment provides the best compromise, offering the best *KGE* for many stations (35%) while minimizing the difference in *KGE* with the best experiment for the remaining stations. Since the difference in *KGE* between experiments with α_{MP} of 0.5 and 0.55 is negligible (Fig. 4a), we chose to set α_{MP} to 0.55. Therefore, we will use a α_{MP} of 0.55 in the Fr-MP experiment to compare with the two other experiments (noFr et Fr).



390

395

400

Figure 4: Boxplots of streamflow KGE for soil freezing and macropores experiments (Fr-MP) using values of α_{MP} from 0.50 to 0.99 by increments of 0.05 on the Great-Lakes and Saint-Lawrence domain from 1 September 2016 to 31 August 2018 (a). The target value for the KGE is 1. Map showing the value of α_{MP} which results in the best KGE for each station (b). When two experiments with different α_{MP} result in the same KGE on a given station, the experiment with the lowest α_{MP} is shown on the map. Only stations for which at least one experiment results in a NSE greater than 0 or a KGE greater than -0.41 (see Sect. 2.4.1) are shown in (a) and (b) (435 stations). Boxplots of the differences in KGE between experiments with each value of α_{MP} and the experiment resulting in the best KGE at stations for which the given experiment does not result in the best KGE (number and percentage of station shown above each boxplot) (c). The lower and upper limits of the boxes on (a) and (c) correspond to the first and third quartile, the median is shown by a horizontal black ($\alpha_{MP} = 0.50$ to 0.70) or white ($\alpha_{MP} = 0.75$ to 0.99) line and the lower and upper whiskers represent the fifth and ninety-fifth percentiles while the outliers are not shown.

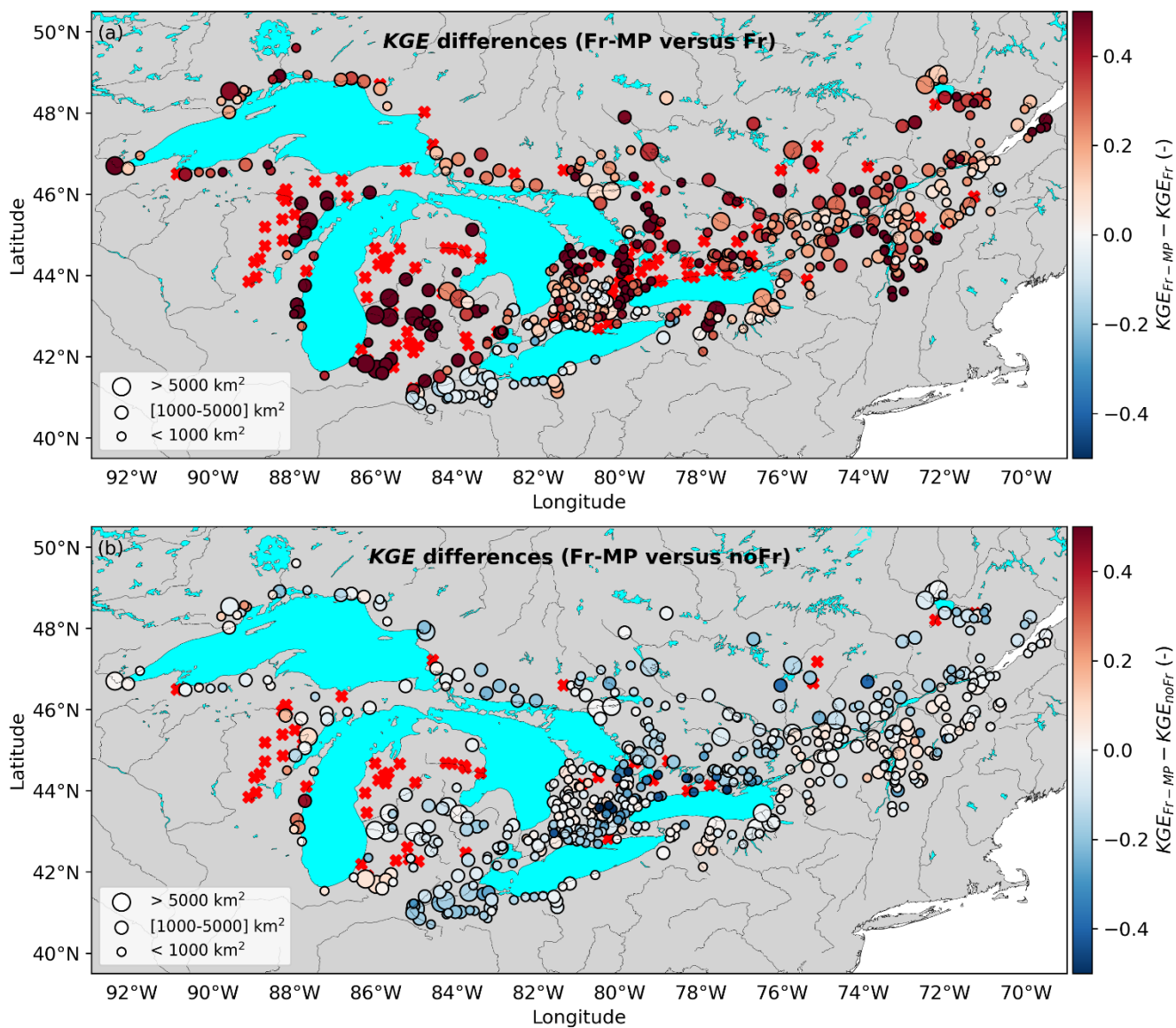


3.3 Hydrologic impact of soil freezing with macropores

Activating macropores in the soil freezing module (Fr-MP) results in a major improvement of the *KGE* across the GLSL domain, as illustrated in Fig. 5a. Improvements in *KGE* are observed at 88% of the stations for which a comparison was established, resulting in an increase in the median *KGE* of 0.28. Representing macropores enhances infiltration into frozen ground, reducing overestimation of peak flow and improving the *NSE* and *KGE* criteria (see Eq. 11 and 12). Stations at which the Fr-MP experiment decreases the *KGE* are located in agricultural areas, where runoff is more prevalent than infiltration and high, reactive streamflow peaks are observed. Note that only 79% of stations are included in the Fr vs. Fr-MP analysis because the Fr-MP experiment more often fails to meet the *NSE* or *KGE* criteria than the noFr experiment (noFr; see Sect. 2.4.1). Compared to the noFr experiment, the Fr-MP experiment generally degrades the *KGE* across the GLSL domain (degradation at 72% of the stations; $\Delta KGE = -0.07$). Unlike the Fr experiment, the Fr-MP experiment results in fairly minor *KGE* degradations with a $\Delta KGE < -0.5$. only at 4 stations (< 1%). Consequently, more stations show improvements in *KGE* from the Fr-MP experiment than from the Fr experiment, when compared to the noFr experiment. These improvements are concentrated in the southern part of Lake Ontario, the Saint-Lawrence River valley, and the vicinity of Lake Michigan. These regions encompass catchments with mixed surfaces of crops, grass, and forests (Fig. 2).

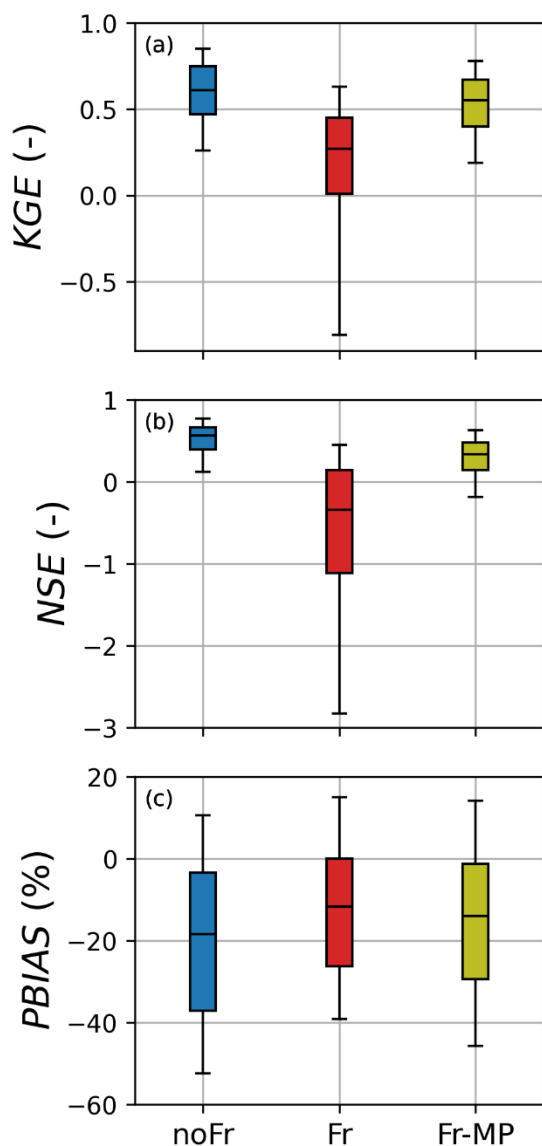
Figure 6 shows the boxplots of *KGE*, *NSE* and *PBIAS* for each of the three experiments. This comparison includes the 521 stations for which at least one experiment between the three resulted in an *NSE* greater than 0 or a *KGE* greater than -0.41. The noFr experiment produced the best results, while the Fr experiment produced the worst results in terms of *KGE* and *NSE*. While the Fr-MP experiment does not outperform the noFr experiment, implementing macropores considerably improves the *KGE* and *NSE* metrics compared to the Fr experiment. These results align with those in Fig. 5.

In contrast to the *KGE* and *NSE*, the noFr and the Fr experiments result in the largest and the smallest negative biases, respectively (Fig. 6c). This is expected as soil freezing limits infiltration and increases runoff. More interesting, however, is that the *PBIAS* of the Fr-MP experiment is nearly equal to that of the Fr experiment. It demonstrates that the large improvements in *KGE* and *NSE* resulting from the addition of the macropore configuration to the soil freezing module do not exacerbate the general underestimation of streamflow.



425

Figure 5: Same as Fig. 3 but for the differences between freezing with macropores (Fr-MP) and soil freezing (Fr) experiments in (a) and between Fr-MP and the experiment without soil freezing (noFr) in (b).



430 **Figure 6: Boxplots of streamflow performances (*KGE* (a), *NSE* (b) and *PBIAS* (c)) for the three configurations (noFr, Fr, Fr-MP) in the Great-Lakes and Saint-Lawrence domain for the 2016-2021 evaluation period. Details on boxplot representation are given in the legend of Fig. 4. The target value for the *KGE* and *NSE* is 1.0 while the target value for the *PBIAS* is 0.0.**

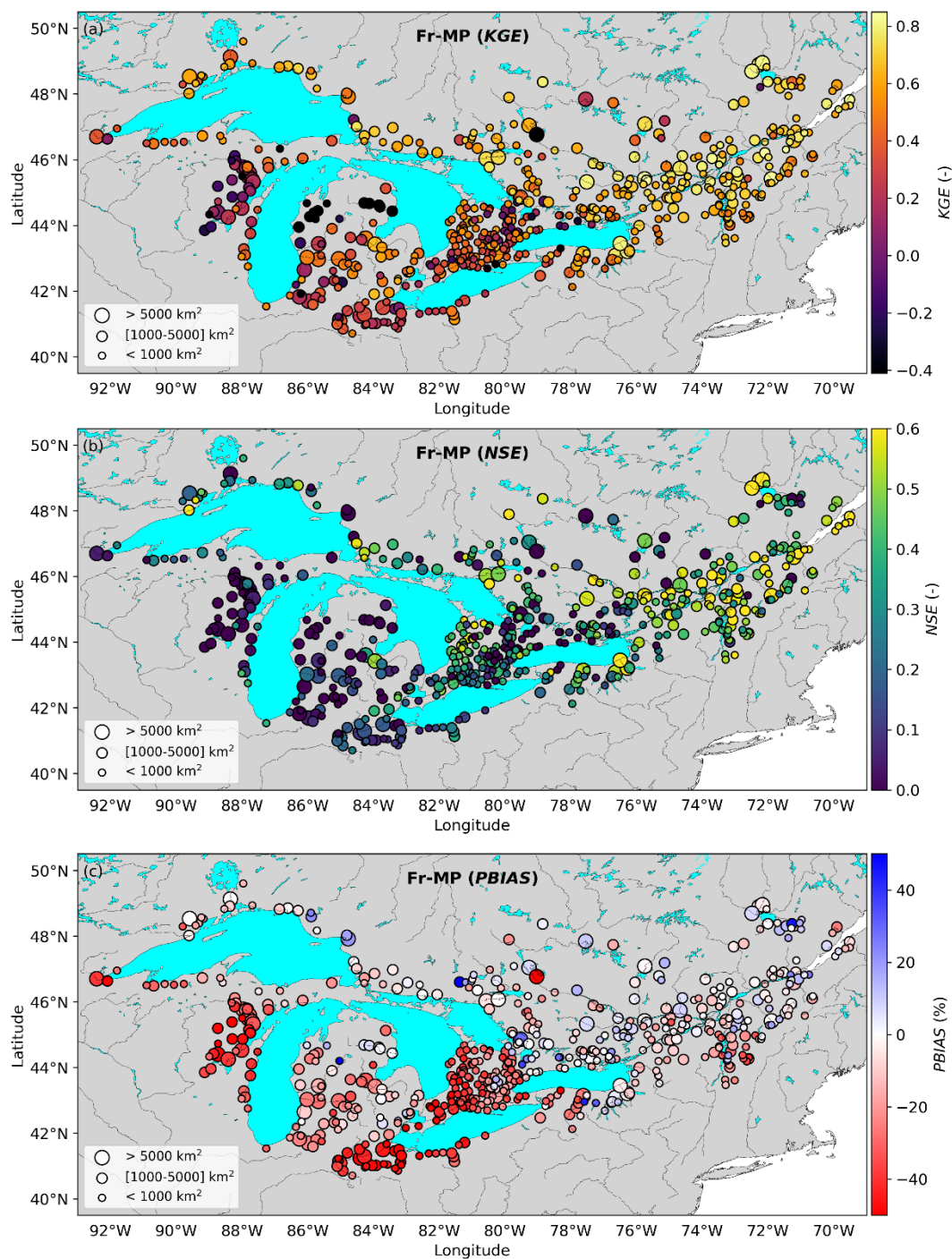
A clear spatial pattern resulting from the Fr-MP experiment emerges from the score maps of *KGE*, *NSE* and *PBIAS* over the GLSL domain (Fig. 7). The performance of Fr-MP is the highest for each of the three metrics in the Saint-Lawrence valley and north of Lake Superior and Lake Huron, where forested land covers prevail (evergreen and mixed forests; Fig. 2). The *KGE* is greater than 0.8 (yellow dots on Fig. 7a) in that area while it falls to 0.4 in the region between Lake Huron and Lake Ontario and East of Lake Erie. The worst *KGE* scores are obtained in the northern region between Lake Michigan and Lake Huron, and West of Lake Michigan, where the *KGE* is lower than 0 at many stations. Note that the same pattern results from

435



the noFr and Fr experiments (Fig. S1 in the Supplementary Materials), which suggests that the model performs better in forested, natural environments than in agricultural and urban areas, regardless of the activation of soil freezing or macropores. 440 The spatial pattern of the *NSE* closely follows that of the *KGE*, with the best results obtained in the northern and eastern parts of the GLSL domain ($NSE > 0.5$), and the worst scores obtained in the southern and western parts of the domain ($NSE < 0.2$). The similarity between the *KGE* and the *NSE* maps implies that the *KGE* can be explained by its variability component at most stations. Additionally, the catchments for which Fr-MP performs best in terms of *NSE* are located at higher latitudes. The streamflow regime in these areas are generally characterized by spring snowmelt rather than by several mid-winter events, 445 compared to stations located in the south of the domain. A high *NSE* in these conditions suggests that Fr-MP reasonably reproduces the amplitude and timing of peak spring flow given that the calculation of the *NSE* attributes gives more weight to large values (Eq. 11).

In line with the *KGE* and *NSE* criteria, the absolute *PBIAS* is minimal for many stations located in the Saint-Lawrence Valley and North of Lake Superior and Lake Huron, with absolute values below 10% (pale blue or red on Fig. 7c). In these regions, 450 the Fr-MP experiment overestimates streamflow (blue dots), though it tends to underestimate streamflow elsewhere. This positive bias is attributed to the soil freezing configuration that remains too restrictive to infiltration despite the addition of macropores. Consequently, most stations in the eastern part of the domain, where the bias is positive, are also stations where the Fr-MP degrades the *KGE* compared to noFr (Fig. 5b). The overall negative bias in the rest of the domain can be explained by an underestimation of streamflow during periods of low-flow regime. As the available pore space for liquid water decreases 455 with growing soil ice, lateral flow likely prevails over soil drainage. This reduces the liquid water that contributes to support base flow.



460 **Figure 7: Maps of the Great-Lakes and Saint-Lawrence domain showing the *KGE* (a), the *NSE* (b) and the *PBIAS* (c) at each station for the Fr-MP experiment over the 2016-2021 period. In (a) and (b), a good performance of the model is represented by yellow shades. In (c), underestimation of streamflow is shown by red colors while an overestimation is shown by blue colors. Pale red and blue dots show a low absolute bias in (c).**



3.4 Impact of soil freezing and macropores on streamflow hydrographs flux partitioning

Activating soil freezing and macropores in SVS results in changes in the behavior of simulated hydrographs. Figure 8 illustrates how the modeled streamflow varies between each experiment for three stations representative of different hydrological conditions within the GLSL domain. The Petawawa River flows eastward and drains a large forested area. The Saint-François River, that flows northward and drains an area almost twice as large as for the Petawawa River, is characterized by various surface types including crops, grassland and forests. The Thames River is located in Southern Ontario and drains a large agricultural catchment. In the Supplementary Materials, we also present hydrographs from three additional stations that drain large natural areas. The Richelieu River and the Ottawa River drain the two largest catchments in the GLSL domain, and the Mistassini River flows through a large boreal catchment. Mistassini River is also one of the northernmost stations in the domain.

Across all catchments, the incorporation of macropores into the soil freezing scheme attenuates discharge peaks under frozen soil conditions while maintaining greater responsiveness than the experiment without soil freezing. For the Petawawa River (Fig. 8a and Fig. S2), Fr-MP produces a twofold increase in KGE relative to the Fr experiment, yet slightly underperforms compared to the noFr experiment ($\Delta KGE = -0.04$). This minor discrepancy in KGE is attributed to erroneous simulations of mid-winter streamflow peaks and a steep recession limb in the spring hydrograph. In the case of the Saint-François River (Fig. 8b), where observed streamflow is slightly more responsive to mid-winter events, Fr-MP substantially improves KGE compared to Fr, achieving a score of 0.84, slightly surpassing noFr. Conversely, for the Thames River (Fig. 8c), which features multiple winter peaks, enhanced infiltration via macropores leads to a slight degradation in KGE relative to Fr ($\Delta KGE = -0.04$), though it remains a moderate improvement over noFr ($\Delta KGE = 0.07$). The comparatively lower performance of Fr-MP at the Thames River may be mitigated by increasing the coefficients for ploughing and tile drainage effects (Gaborit et al., 2025). The hydrographs from the three catchments presented in Fig. S2 show similar results. Fr-MP clearly improves the performance compared to Fr and results in similar or slightly degraded performance compared to noFr. It demonstrates that incorporating macropores into the soil freezing scheme of SVS improves streamflow simulations for catchments of various landscapes and sizes.

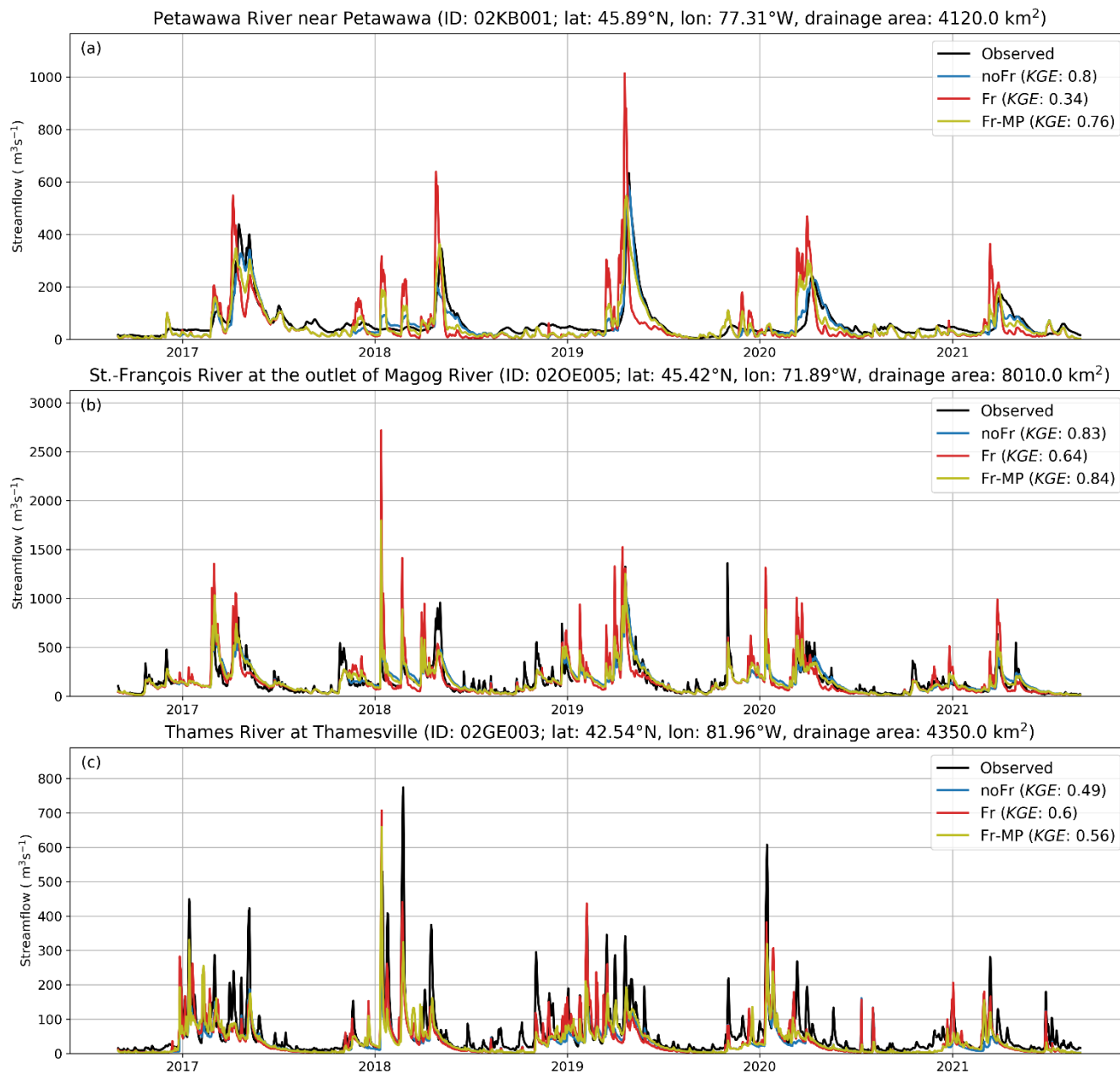


Figure 8: Observed and simulated streamflow of the Petawawa River (station ID: 02KB001) (a), the Saint-François River (station ID: 02OE005) (b) and the Thames River (station ID: 02GE003) (c) for the 2016-2021 evaluation period. Simulations of the no freezing experiment (noFr) are in blue, the soil freezing experiment (Fr) in red and the soil freezing with macropores (Fr-MP) in yellow.

490 Figure 9 shows an example of how each surface hydrological flux is simulated under each of the three model configurations. In this example, we present the case of the Moira River at the station near Foxboro (NSRPS station ID: 02HL001). The Moira River flows through a natural, mostly forested catchment located north of Lake Ontario. During the period from 2016 to 2021,

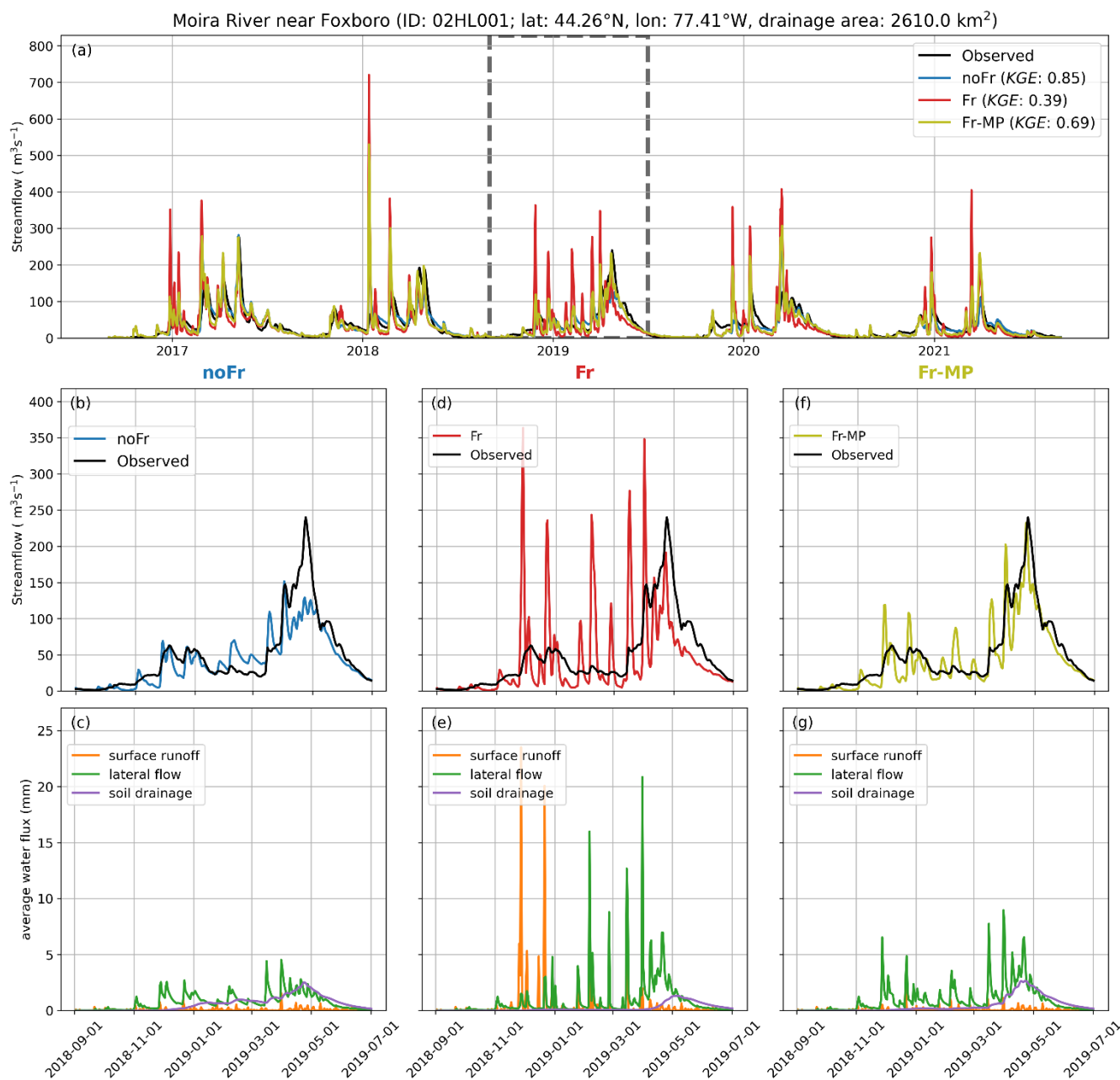


the peak flow varied between $100 \text{ m}^3 \text{ s}^{-1}$ (in 2021) and $275 \text{ m}^3 \text{ s}^{-1}$ (in 2017), while the low flow approached $0 \text{ m}^3 \text{ s}^{-1}$ every summer (Fig. 9a). All three model configurations have the tendency of simulating peaks of discharge in winter that are not
495 observed at the gauging station. This could be explained by the presence of numerous wetlands and meanders in the area, which have the effect of attenuating runoff peaks during rain and thaw events. These processes are not yet fully represented in Watrouite.

A detailed examination of the September 2018 to June 2019 period reveals distinct differences in streamflow simulations at station 02HL001 across the model configurations. Relative to the Fr and Fr-MP experiments, the noFr configuration produces
500 the highest winter base flow, yet exhibits the most significant underestimation of spring peak flow (Fig. 9b). The large base flow is attributed to persistent soil drainage, driven by continuous infiltration and percolation (Fig. 9c, purple curve). As a result, the reduced surface runoff and lateral flow in spring (orange and green curves) constrain the magnitude of spring freshets for this experiment and this station.

In contrast, the Fr experiment displays markedly different hydrograph dynamics, featuring frequent high-magnitude discharge
505 events in winter and spring alongside low base flow (Fig. 9d). This behavior is attributed to early-winter surface runoff peaks (Fig. 9e, orange curve) followed by lateral flow peaks from January onward (green curve). Soil ice accumulation in near-surface layers during early winter reduces effective porosity, thereby enhancing saturation-excess runoff generation (Alavi et al., 2016). Subsequently, as the freezing front advances deeper into the soil column, increased saturation in subsurface layers forces excess water to discharge as lateral flow. As a result, percolation to the deep soil layers is negligible, effectively limiting
510 the drainage contribution to base flow (Fig. 9e, purple curve).

The inclusion of macropores in the soil freezing module represents an effective compromise between the noFr and Fr configurations. Specifically, Fr-MP attenuates winter peaks in favor of base flow and yields a more accurate simulation of the spring freshet compared to Fr (Fig. 9f). Mitigating runoff caused by surface layer saturation reduces the surface runoff component (Fig. 9g, orange curve) and facilitates water redistribution into lower soil layers. Furthermore, percolation is
515 promoted when the macropore activation criterion ($\alpha_{MP} > 0.55$) is satisfied. This results in dampened lateral flow peaks during winter and spring, coupled with an increased contribution of soil drainage to the spring peak flow (Fig. 9g, green and purple curves). Yet the Fr-MP experiment still leads to hydrologic behavior that is too flashy for this station, but as explained earlier, this could be due to the fact that the effects of the meanders and wetlands along this river are not currently well captured by the Watrouite model used here.



520

Figure 9: Observed and simulated streamflow at the Moira River (station ID: 02HL001) for the 2016-2021 evaluation period with the specific year 2018-2019 identified with the dashed line (a). The streamflow simulated with the noFr, Fr and Fr-MP configurations for the 2018-2019 year is shown against the observed streamflow on (b), (d) and (f), respectively. Water fluxes from SVS (surface runoff, lateral flow and soil drainage) averaged over the drainage area of station 02HL001 for the year 2018-2019 period are presented for each experiment on (c), (e) and (g).

525



3.5 Evaluation of near-surface meteorology and depth of frozen soil

Given the upcoming implementation of the soil freezing scheme of SVS within the operational framework of ECCC for numerical weather predictions, it is critical to evaluate how the proposed configuration affects surface variables. Table 1 details the changes in performance metrics ($\Delta BIAS$, $\Delta RMSE$ and ΔSTD) between the Fr-MP and noFr experiments for near-surface dewpoint (TD) and air (TT) temperatures, analyzed both over the full period and seasonally. The inclusion of the soil freezing configuration with macropores results in either neutral performance or slight improvements across all metrics. Notably, improvements are greater for TT than for TD , and are more important in winter compared to spring, while remaining neutral in summer. Similar results comparing Fr and noFr (Supplementary Material, Table S1) suggest that these benefits stem primarily from the activation of the soil freezing module rather than the macropores. Consequently, the new configuration does not compromise the quality of surface variable estimation. Rather, it provides slight enhancements under conditions favorable to soil freezing.

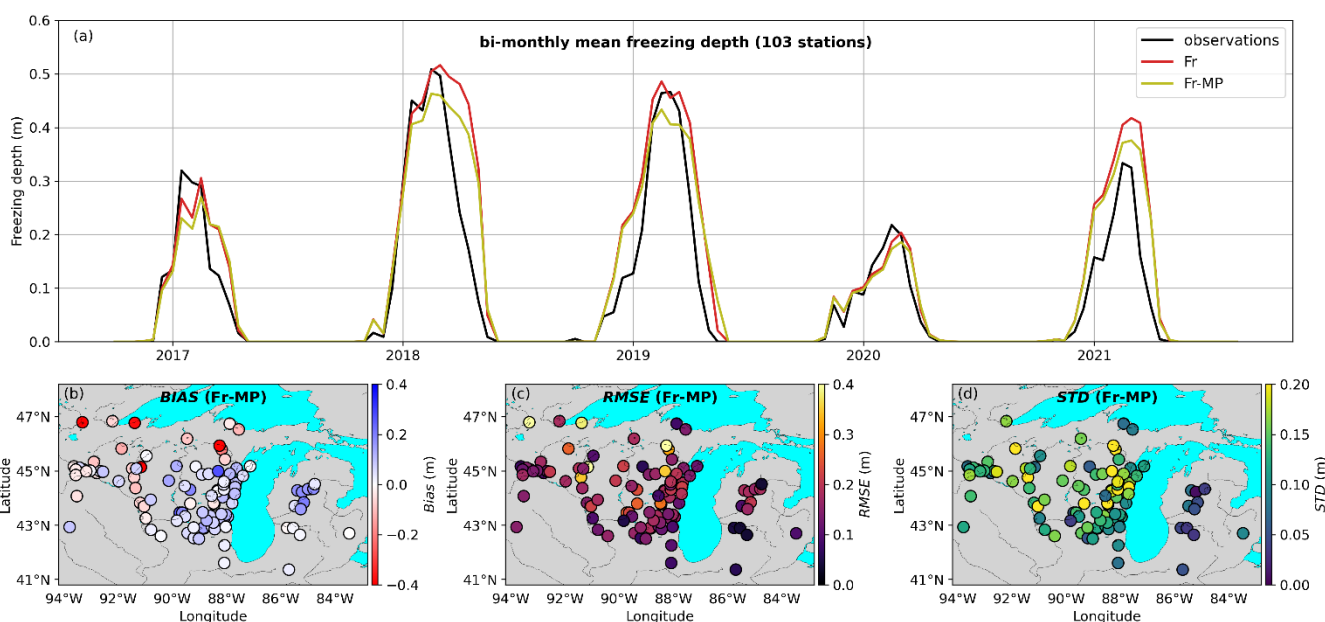
	period/ variable	Full period 2016-09-01 to 2021-08-31	Winter 11/01 to 02/28	Spring 03/01 to 06/30	Summer 07/01 to 10/31
$\Delta BIAS$ (°C)	TD	0.021	0.011	0.03	0
	TT	0.026	0.052	0.024	0.001
$\Delta RMSE$ (°C)	TD	0.008	0.007	0.015	0
	TT	0.016	0.019	0.015	0.001
ΔSTD (°C)	TD	0.001	0.004	0.002	0
	TT	0.008	0.007	0.01	0.001

Table 1: Differences of the bias ($BIAS$), root mean square error ($RMSE$) and standard deviation of the error (STD) for the 2 m dew point temperature (TD) and the 2 m air temperature (TT) between the soil freezing with macropores experiment (Fr-MP) and the experiment without soil freezing (noFr). The performances are evaluated over the full period (from 1 September 2016 to 31 August 2021) and seasonally with winter period spanning from 1 November to 28 February, spring period from 1 March to 30 June and summer period from 1 July to 31 October. Positive values greater than 0.01°C are shown in bold and represent an improvement of the Fr-MP experiment compared to noFr.

The integration of soil freezing into SVS is particularly valuable, as it yields additional output variables of potential interest for external users. It is therefore imperative to assess the accuracy of soil freezing simulations relative to observational data. Figure 10a compares the observed freezing depth, averaged across 103 stations in the central U.S., with results from the Fr and Fr-MP experiments. Both configurations show strong agreement with observations regarding amplitude and interannual variability. The freezing depth simulated by Fr-MP is slightly reduced compared to Fr. This is likely explained by higher water retention in deep soil layers in the Fr-MP configuration, resulting from enhanced infiltration. Consequently, the increased soil moisture imposes a higher energy requirement to freeze the liquid water content of a given layer. Figures 10b–d illustrate the spatial distribution of the 103 stations across the central U.S., with the $BIAS$, $RMSE$, and STD of the Fr-MP experiment represented by color gradients. At most stations, Fr-MP overestimates freezing depth (blue dots in Fig.



10b), except for a distinct cluster in the northern region. These stations correspond to the highest *RMSE* values, though not necessarily to the highest *STD*, implying a consistent underestimation of freezing depth throughout winter and spring. In general, stations where Fr-MP overestimates freezing depth coincide with low *RMSE* values (< 0.15 m), which indicate that Fr-MP is a reliable predictor of freezing depth. However, locations with higher *STD* values exhibit a greater deviation between the model and the observations and consequently a large temporal variability. A similar spatial pattern is observed for the Fr experiment (see Fig. S3 in the Supplementary Materials).



560 **Figure 10: Bi-monthly mean of freezing depth for 103 stations located in the central US from 2016 to 2021 with observations shown in black and soil freezing (Fr) and soil freezing with macropores (Fr-MP) simulations shown in red and yellow, respectively (a). The *BIAS*, *RMSE* and standard deviation (*STD*) at each station over the 2016-2021 period for the Fr-MP experiment are respectively shown in (b), (c) and (d).**

4 Discussion

565 In the current study, we present an updated soil freezing scheme for the SVS land surface model that includes a conceptual representation of macropores designed to enhance infiltration in the presence of soil ice. Here, we compare our performance against similar large-scale land surface modeling studies and outline the limitations of both our approach and the experimental modeling setup.

4.1 Comparison with other studies

570 Koren et al. (2014) assessed the impact of a physically-based modified version of the Sacramento Soil Moisture Accounting model (SAC-SMA) to account for the effect of frozen soil on runoff dynamics in 11 large U.S. Midwest catchments. In this



approach, the effect of ice on the increase in the soil particle-water contact surface is considered in the calculation of a reduced $K_{sat,v}$, which is later used in the SAT-SMA model to estimate runoff generation under frozen soil conditions. This modification resulted in an improved representation of winter and spring hydrograph peaks compared to non-frozen conditions, which contrasts with our findings where the noFr experiment outperformed Fr over the GLSL domain. This divergence is likely attributable to the use of an empirical ice-impedance factor in SVS to impede soil water flow, which is more restrictive to infiltration than the parameterization from Koren et al. (2014). The ice-impedance configuration used in SVS is the same as the one used in the CLASS land surface model (Ganji et al., 2017), which is based on a silty clay loam site in Saskatchewan and derived from Zhao and Gray (1997). The limitations of using such impedance factors to restrict frozen ground infiltration are well documented by Kurylyk and Watanabe (2013).

Ganji et al. (2017) performed a streamflow evaluation of the Canadian Land Surface Scheme (CLASS; Verseghy, 2008) coupled with Watroute (Kouwen, 2010) across 12 catchments in Québec's boreal, subarctic, and arctic regions. They reported improved agreement with observations when the impedance factor (same as in SVS) was tuned to be more restrictive but with a dual-domain infiltration configuration (Niu and Yang, 2006). In another study, Agnihotri et al. (2023) tested various frozen soil hydraulic property schemes within Noah-MP in the Mississippi River basin, finding that streamflow simulations were also improved using the Niu and Yang (2006) configuration but without any ice-impedance factor. Both Ganji et al. (2017) and Agnihotri et al. (2023) obtained optimal results using configurations that facilitate infiltration into frozen ground. This aligns with our finding that activating the macropore configuration in SVS enhances infiltration and improves streamflow simulations. Since these studies and ours cover diverse geographical domains, it suggests that permitting infiltration into frozen soil is critical for accurate large-scale hydrological modeling. Notably, we achieved performance metrics comparable to Agnihotri et al. (2023) with a median KGE of 0.55 without a dual-domain approach. This indicates that applying ice impedance only when liquid water occupies a limited fraction of pore space ($W < 0.55 W_{sat}$) is an effective strategy within SVS to enhance frozen ground infiltration. Although the studies from Ganji et al. (2017), Agnihotri et al. (2023) and ours cover different cold geographical domains, it has been suggested that in permafrost-dominated regions, infiltration should be restricted in LSS to better simulate streamflow (Swenson et al., 2012).

4.2 Limitations

In the proposed approach, macropore flow is triggered when the liquid water content of a soil layer surpasses a sensitivity analysis-derived threshold derived, which is supported by empirical evidence (Alaoui, 2015; Bauer et al., 2025). This approach does not currently rely on land surface characteristics to modulate infiltration, despite well-documented effects of soil texture and land cover on the presence of macropores and their effect frozen ground infiltration (Ala-Aho et al., 2021; Jarvis, 2007; Mohammed et al., 2019; Zhang et al., 2021). In the context of SVS applied in the Great-Lakes and Saint-Lawrence domain, tests using a soil-texture sensitive parameter failed to outperform the macropore activation formulation based on single threshold value. This approach may be revised when applying the model across Canada. Furthermore, attempts to increase vertical hydraulic conductivity ($K_{sat,v}$) to promote preferential flow resulted in numerical instabilities, attributed to the reliance



605 of the SVS vertical flux scheme on Darcian flow (Alavi et al., 2016). Therefore, a comprehensive reformulation of the soil water transfer module is necessary to accurately represent preferential macropore flow under frozen soil conditions.

Certain limitations are inherent to the SVS soil freezing scheme. While modifications were introduced to the soil thermal regime formulation of Amani et al. (2025) to better represent freezing depth, the existing SVS soil freezing module retains significant simplifications. These include the use of the Hayashi et al. (2007) heat conduction algorithm and the neglect of
610 freezing point depression. Furthermore, SVS employs a single-layer snowpack representation whose thermal regime is based on a force-restore scheme (Leonardini et al., 2021). These simplifications constrain the simulation of soil temperature evolution and the associated soil water phase changes. Recently, SVS version 2.0 (SVS2) was released (Vionnet et al., 2025), featuring completely reformulated schemes for soil freezing and snowpack evolution. Comparative research is ongoing to evaluate both SVS versions focusing on frozen ground infiltration.

615 Streamflow simulations under frozen soil conditions are governed by the parameterization of soil water fluxes in SVS. Surface runoff and lateral flow are partially generated via a subgrid-scale interflow parameterization (Soulis et al., 2000). This mechanism was initially parametrized in SVS to represent subsurface flow but also applies to the surface soil layer by configuration. Its impact on surface runoff under unfrozen soil conditions is negligible but was found to be major in the presence of soil ice in the topmost soil layer. Therefore, in the Fr-MP configuration, we chose to disable the subgrid-scale
620 interflow routine at the surface to increase frozen soil infiltration. Furthermore, the near-surface anisotropy ratio ($K_{sat,h}/K_{sat,v}$) is of the order of 1000, a magnitude that strongly promotes lateral flow over infiltration. Current efforts focus on refining the lateral flow formulation in SVS by incorporating new anisotropy estimations based on Brooks et al. (2004) and Decharme et al. (2013).

Finally, the Watroute routing model lacks groundwater reservoir exchanges and has known limitations in simulating flow
625 within meandering regions and wetland areas (Gaborit et al., 2025). This likely contributes to the poor performance observed in the region bounded by the five Great Lakes (Fig. 7). The envisioned transition in NSRPS from Watroute to the Raven routing scheme (Craig et al., 2020) in the coming years may help alleviate these issues.

5 Conclusion

In this work, we proposed a conceptual approach to parameterize the effect of macropores on frozen soil infiltration within
630 SVS, the land surface component of the GEM-Hydro hydrometeorological modelling platform. The evaluation, performed against observations from over 580 hydrometric stations in the Great-Lakes and Saint-Lawrence domain over five years, indicates that enhancing infiltration under frozen soil conditions yields improved streamflow performances at 88% of the stations for which a comparison was performed with the median KGE increasing by 0.28. The improved configuration utilizes unimpeded hydraulic conductivity when liquid water content surpasses a specific threshold relative to available pore space.
635 This mechanism promotes soil drainage at the expense of surface runoff and lateral flow, thereby improving the simulation of winter flow and spring freshet. The new soil freezing scheme including enhanced macropore infiltration further provides an



accurate freezing depth estimation without compromising performance for near-surface variables (dew point and air temperature).

Our findings demonstrate that the updated soil freezing scheme is capable of accurately estimating streamflow across large hydrological domains. Future work will focus on evaluating this improved SVS version within GEM-Hydro across Canada. This assessment is a prerequisite for the operational implementation of the soil freezing formulation in the NSRPS. Ultimately, improving the representation of soil freezing and thawing in SVS is a critical step toward its adoption as the operational land surface scheme within the GEM-based numerical weather prediction systems of ECCC.

Code availability. The version of the SVS code integrated within the Surface Prediction System (SPS) of ECCC and the modified routines that include the new configuration of macropores are freely available in a permanent repository: <https://doi.org/10.5281/zenodo.18664365>. The Watroute routing scheme is available in the MESH official repository: <https://github.com/MESH-Model/MESH-Releases>. Note that the Watroute version included in MESH can moreover not be run in a standalone mode, but only together with the SVS land-surface scheme. The Watroute version used internally at ECCC cannot yet be run outside of ECCC infrastructure. It is therefore not yet possible to exactly replicate the GEM-Hydro simulations described here, outside of ECCC informatic infrastructure. Finally, the Canadian Surface Reanalysis forcing data used in this study can be downloaded here: <https://hpfx.collab.science.gc.ca/~scar700/rcas-casr/index.html>.

Author contributions. BB, VV, ÉG and VF designed the study. ÉG provided the GEM-Hydro setup, guidance with running the GEM-Hydro model in open-loop mode, guidance with using python scripts originally developed by VV and ÉG to perform the streamflow evaluations, and guidance with using ECCC's internal "EMET" tool to perform the evaluation of the surface variables. VV developed the package used for the evaluation of the depth of frozen soil. BB performed and evaluated the simulations after improving the evaluation scripts. All authors contributed to analyzing simulation results. BB wrote the manuscript with inputs from all other authors.

Competing interests. The contact author has declared that none of the authors has any competing interest.

Acknowledgements. The authors wish to thank other members of the Numerical Terrestrial Environmental Prediction Research section of the Meteorological Research Division of ECCC for their valuable feedback throughout the work. AI tools were used in the preparation of this manuscript for revising text for flow and grammar.

References

Agnihotri, J., Behrangi, A., Tavakoly, A., Geheran, M., Farmani, M. A., and Niu, G.: Higher Frozen Soil Permeability Represented in a Hydrological Model Improves Spring Streamflow Prediction From River Basin to Continental Scales, *Water Resour. Res.*, 59, e2022WR033075, <https://doi.org/10.1029/2022WR033075>, 2023.



- Ala-Aho, P., Autio, A., Bhattacharjee, J., Isokangas, E., Kujala, K., Marttila, H., Menberu, M., Meriö, L.-J., Postila, H., Rauhala, A., Ronkanen, A.-K., Rossi, P. M., Saari, M., Haghighi, A. T., and Kløve, B.: What conditions favor the influence of seasonally frozen ground on hydrological partitioning? A systematic review, *Environ. Res. Lett.*, 16, 043008, <https://doi.org/10.1088/1748-9326/abe82c>, 2021.
- 670 Alaoui, A.: Modelling susceptibility of grassland soil to macropore flow, *J. Hydrol.*, 525, 536–546, <https://doi.org/10.1016/j.jhydrol.2015.04.016>, 2015.
- Alavi, N., Bélair, S., Fortin, V., Zhang, S., Husain, S. Z., Carrera, M. L., and Abrahamowicz, M.: Warm Season Evaluation of Soil Moisture Prediction in the Soil, Vegetation, and Snow (SVS) Scheme, *J. Hydrometeorol.*, 17, 2315–2332, <https://doi.org/10.1175/jhm-d-15-0189.1>, 2016.
- 675 Amani, A., Boucher, M.-A., Cabral, A. R., Vionnet, V., and Gaborit, É.: Cold Climates, Complex Hydrology: Can A Land Surface Model Accurately Simulate Deep Percolation?, *Hydrol. Earth Syst. Sci.*, 2445–2465, <https://doi.org/doi.org/10.5194/hess-29-2445-2025>, 2025.
- Appels, W. M., Coles, A. E., and McDonnell, J. J.: Infiltration into frozen soil: From core-scale dynamics to hillslope-scale connectivity, *Hydrol. Processes*, 32, 66–79, <https://doi.org/10.1002/hyp.11399>, 2018.
- 680 Barredo, J. I.: Major flood disasters in Europe: 1950–2005, *Nat. Hazards*, 42, 125–148, <https://doi.org/10.1007/s11069-006-9065-2>, 2007.
- Bauer, J., Müller, S., Heinze, T., Khanahmadi Bafghi, H., and Baselt, I.: Thermohydraulic Experiments on Water Infiltration in Frozen Slopes: The Role of Macropores and Initial Water Content, *EGUsphere* [preprint], <https://doi.org/10.5194/egusphere-2025-5473>, 5 December 2025.
- 685 Bernier, N. B., Bélair, S., Bilodeau, B., and Tong, L.: Near-Surface and Land Surface Forecast System of the Vancouver 2010 Winter Olympic and Paralympic Games, *J. Hydrometeorol.*, 12, 508–530, <https://doi.org/10.1175/2011JHM1250.1>, 2011.
- Beven, K. and Germann, P.: Macropores and water flow in soils revisited: REVIEW, *Water Resour. Res.*, 49, 3071–3092, <https://doi.org/10.1002/wrcr.20156>, 2013.
- Boone, A., Masson, V., Meyers, T., and Noilhan, J.: The Influence of the Inclusion of Soil Freezing on Simulations by a Soil–Vegetation–Atmosphere Transfer Scheme, *J. Appl. Meteorol.*, 39, 1544–1569, [https://doi.org/10.1175/1520-0450\(2000\)039<1544:TIOTIO>2.0.CO;2](https://doi.org/10.1175/1520-0450(2000)039<1544:TIOTIO>2.0.CO;2), 2000.
- 690 Bouchard, B., Nadeau, D. F., Domine, F., Anctil, F., Jonas, T., and Tremblay, É.: How does a warm and low-snow winter impact the snow cover dynamics in a humid and discontinuous boreal forest? Insights from observations and modeling in eastern Canada, *Hydrol. Earth Syst. Sci.*, 28, 2745–2765, <https://doi.org/10.5194/hess-28-2745-2024>, 2024.
- 695 Boussetta, S., Balsamo, G., Arduini, G., Dutra, E., McNorton, J., Choulga, M., Agustí-Panareda, A., Beljaars, A., Wedi, N., Munõz-Sabater, J., De Rosnay, P., Sandu, I., Hadade, I., Carver, G., Mazzetti, C., Prudhomme, C., Yamazaki, D., and Zsoter, E.: ECLand: The ECMWF Land Surface Modelling System, *Atmopshere*, 12, 723, <https://doi.org/10.3390/atmos12060723>, 2021.



- Brooks, E. S., Boll, J., and McDaniel, P. A.: A hillslope-scale experiment to measure lateral saturated hydraulic conductivity, *Water Resour. Res.*, 40, 2003WR002858, <https://doi.org/10.1029/2003WR002858>, 2004.
- Burt, T. P. and Williams, P. J.: Hydraulic conductivity in frozen soils, *Earth Surf. Process.*, 1, 349–360, <https://doi.org/10.1002/esp.3290010404>, 1976.
- Campbell, J. L., Soggi, A. M., and Templer, P. H.: Increased nitrogen leaching following soil freezing is due to decreased root uptake in a northern hardwood forest, *Global Change Biol.*, 20, 2663–2673, <https://doi.org/10.1111/gcb.12532>, 2014.
- 705 Carrera, M. L., Bélair, S., and Bilodeau, B.: The Canadian Land Data Assimilation System (CaLDAS): Description and Synthetic Evaluation Study, *J. Hydrometeorol.*, 16, 1293–1314, <https://doi.org/10.1175/JHM-D-14-0089.1>, 2015.
- Changwei, X. and Gough, W. A.: A Simple Thaw-Freeze Algorithm for a Multi-Layered Soil using the Stefan Equation, *Permafr. Periglac. Process.*, 24, 252–260, <https://doi.org/10.1002/ppp.1770>, 2013.
- Clapp, R. B. and Hornberger, G. M.: Empirical equations for some soil hydraulic properties, *Water Resour. Res.*, 14, 601–604, <https://doi.org/10.1029/WR014i004p00601>, 1978.
- 710 Covino, T.: Hydrologic connectivity as a framework for understanding biogeochemical flux through watersheds and along fluvial networks, *J. Geomorph.*, 277, 133–144, <https://doi.org/10.1016/j.geomorph.2016.09.030>, 2017.
- Craig, J. R., Brown, G., Chlumsky, R., Jenkinson, R. W., Jost, G., Lee, K., Mai, J., Serrer, M., Sgro, N., Shafii, M., Snowdon, A. P., and Tolson, B. A.: Flexible watershed simulation with the Raven hydrological modelling framework, *Environ. Model. Software*, 129, 104728, <https://doi.org/10.1016/j.envsoft.2020.104728>, 2020.
- 715 Dall’Amico, M., Endrizzi, S., Gruber, S., and Rigon, R.: A robust and energy-conserving model of freezing variably-saturated soil, *The Cryosphere*, 5, 469–484, <https://doi.org/10.5194/tc-5-469-2011>, 2011.
- Decharme, B., Martin, E., and Faroux, S.: Reconciling soil thermal and hydrological lower boundary conditions in land surface models, *J. Geophys. Res.: Atmos.*, 118, 7819–7834, <https://doi.org/10.1002/jgrd.50631>, 2013.
- 720 Demand, D., Selker, J. S., and Weiler, M.: Influences of Macropores on Infiltration into Seasonally Frozen Soil, *Vadose Zone J.*, 18, 1–14, <https://doi.org/10.2136/vzj2018.08.0147>, 2019.
- Durnford, D., Fortin, V., Smith, G., Carrera, M., Deacu, D., Dupont, F., Gaborit, É., Gauthier, N., Garnaud, C., Vionnet, V., Lan Shin, Y., Lespinas, F., Bekcic, B., and Sétigui, K.: Hydrological prediction systems at Environment and Climate Change Canada, American Meteorological Society Annual Meeting, Online, 10-15 January 2021, 2021AMS10183559D, 2021.
- 725 Flerchinger, G. N. and Saxton, K. E.: Simultaneous Heat and Water Model of a Freezing Snow-Residue-Soil System I. Theory and Development, *Transactions of the ASAE*, 32, 0565–0571, <https://doi.org/10.13031/2013.31040>, 1989.
- Fortin, V., Roy, G., Donaldson, N., and Mahidjiba, A.: Assimilation of radar quantitative precipitation estimations in the Canadian Precipitation Analysis (CaPA), *J. Hydrol.*, 531, 296–307, <https://doi.org/10.1016/j.jhydrol.2015.08.003>, 2015.
- 730 Gaborit, É., Fortin, V., Xu, X., Seglenieks, F., Tolson, B., Fry, L. M., Hunter, T., Anctil, F., and Gronewold, A. D.: A hydrological prediction system based on the SVS land-surface scheme: efficient calibration of GEM-Hydro for streamflow simulation over the Lake Ontario basin, *Hydrol. Earth Syst. Sci.*, 21, 4825–4839, <https://doi.org/10.5194/hess-21-4825-2017>, 2017.



- Gaborit, É., Fortin, V., and Durnford, D.: On the implementation of the dynamically zoned target release reservoir model in the GEM-Hydro streamflow forecasting system, *Can. J. Civ. Eng.*, 49, 1582–1594, <https://doi.org/10.1139/cjce-2021-0507>, 2022.
- Gaborit, É., Mai, J., Princz, D., Shen, H., Vionnet, V., Tolson, B., and Fortin, V.: Hydrologic outputs generated over the Great Lakes with a calibrated version of the GEM-Hydro model, *Sci. Data*, 12, 127, <https://doi.org/10.1038/s41597-025-04409-x>, 2025.
- Ganji, A., Sushama, L., Versegny, D., and Harvey, R.: On improving cold region hydrological processes in the Canadian Land Surface Scheme, *Theor. Appl. Climatol.*, 127, 45–59, <https://doi.org/10.1007/s00704-015-1618-4>, 2017.
- Gasset, N., Fortin, V., Dimitrijevic, M., Carrera, M., Bilodeau, B., Muncaster, R., Gaborit, É., Roy, G., Pentcheva, N., Bulat, M., Wang, X., Pavlovic, R., Lespinas, F., Khedhaouria, D., and Mai, J.: A 10 km North American precipitation and land-surface reanalysis based on the GEM atmospheric model, *Hydrol. Earth Syst. Sci.*, 25, 4917–4945, <https://doi.org/10.5194/hess-25-4917-2021>, 2021.
- Gasset, N., Khedhaouria, D., Fortin, V., Lauer, A., Dimitrijevic, M., Bulat, M., Pentcheva, N., Wang, X., and Muncaster, R.: Réanalyse canadienne de surface (RCaS-CaSR) version 3.1 d’Environnement et Changement Climatique Canada (ECCC), Symposium Ouranos, Online, 28-29 January, 2025.
- Gray, D. M., Landine, P. G., and Granger, R. J.: Simulating infiltration into frozen Prairie soils in streamflow models, *Can. J. Earth Sci.*, 22, 464–472, <https://doi.org/10.1139/e85-045>, 1985.
- Gronewold, A. D., Do, H. X., Mei, Y., and Stow, C. A.: A Tug-of-War Within the Hydrologic Cycle of a Continental Freshwater Basin, *Geophys. Res. Lett.*, 48, e2020GL090374, <https://doi.org/10.1029/2020GL090374>, 2021.
- Hansson, K., Šimůnek, J., Mizoguchi, M., Lundin, L.-C., and Van Genuchten, M. Th.: Water Flow and Heat Transport in Frozen Soil: Numerical Solution and Freeze–Thaw Applications, *Vadose Zone J.*, 3, 93–704, <https://doi.org/10.2136/vzj2004.0693>, 2005.
- Harlan, R. L.: Analysis of coupled heat-fluid transport in partially frozen soil, *Water Resour. Res.*, 9, 1314–1323, <https://doi.org/10.1029/WR009i005p01314>, 1973.
- Hayashi, M., Goeller, N., Quinton, W. L., and Wright, N.: A simple heat-conduction method for simulating the frost-table depth in hydrological models, *Hydrol. Processes*, 21, 2610–2622, <https://doi.org/10.1002/hyp.6792>, 2007.
- Henry, H. A. L.: Climate change and soil freezing dynamics: historical trends and projected changes, *Clim. Change*, 87, 421–434, <https://doi.org/10.1007/s10584-007-9322-8>, 2008.
- Hersbach, H., Bell, B., Berrisford, P., Hirahara, S., Horányi, A., Muñoz-Sabater, J., Nicolas, J., Peubey, C., Radu, R., Schepers, D., Simmons, A., Soci, C., Abdalla, S., Abellan, X., Balsamo, G., Bechtold, P., Biavati, G., Bidlot, J., Bonavita, M., De Chiara, G., Dahlgren, P., Dee, D., Diamantakis, M., Dragani, R., Flemming, J., Forbes, R., Fuentes, M., Geer, A., Haimberger, L., Healy, S., Hogan, R. J., Hólm, E., Janisková, M., Keeley, S., Laloyaux, P., Lopez, P., Lupu, C., Radnoti, G., De Rosnay, P., Rozum, I., Vamborg, F., Villaume, S., and Thépaut, J.: The ERA5 global reanalysis, *Quart. J. Royal Meteorol. Soc.*, 146, 1999–2049, <https://doi.org/10.1002/qj.3803>, 2020.



- Husain, S. Z., Alavi, N., Bélair, S., Carrera, M., Zhang, S., Fortin, V., Abrahamowicz, M., and Gauthier, N.: The Multibudget Soil, Vegetation, and Snow (SVS) Scheme for Land Surface Parameterization: Offline Warm Season Evaluation, *J. Hydrometeorol.*, 17, 2293–2313, <https://doi.org/10.1175/jhm-d-15-0228.1>, 2016.
- 770 Jame, Y. and Norum, D. I.: Heat and mass transfer in a freezing unsaturated porous medium, *Water Resour. Res.*, 16, 811–819, <https://doi.org/10.1029/WR016i004p00811>, 1980.
- Jarvis, Koestel, J., and Larsbo, M.: Understanding Preferential Flow in the Vadose Zone: Recent Advances and Future Prospects, *Vadose Zone J.*, 15, 1–11, <https://doi.org/10.2136/vzj2016.09.0075>, 2016.
- Jarvis, N. J.: A review of non-equilibrium water flow and solute transport in soil macropores: principles, controlling factors and consequences for water quality, *Eur. J. Soil Sci.*, 71, 279–302, <https://doi.org/10.1111/ejss.12973>, 2007.
- 775 Jean, V., Boucher, M.-A., Frini, A., and Roussel, D.: Fully integrating probabilistic flood forecasts into the decision-making process across southern Quebec, Canada: some factors to consider, *Can. Water Resour. J.*, 49, 153–170, <https://doi.org/10.1080/07011784.2023.2238696>, 2024.
- Kling, H., Fuchs, M., and Paulin, M.: Runoff conditions in the upper Danube basin under an ensemble of climate change scenarios, *J. Hydrol.*, 424–425, 264–277, <https://doi.org/10.1016/j.jhydrol.2012.01.011>, 2012.
- 780 Knobon, W. J. M., Freer, J. E., and Woods, R. A.: Technical note: Inherent benchmark or not? Comparing Nash–Sutcliffe and Kling–Gupta efficiency scores, *Hydrol. Earth Syst. Sci.*, 23, 4323–4331, <https://doi.org/10.5194/hess-23-4323-2019>, 2019.
- Koren, V., Schaake, J., Mitchell, K., Duan, Q. -Y., Chen, F., and Baker, J. M.: A parameterization of snowpack and frozen ground intended for NCEP weather and climate models, *J. Geophys. Res.*, 104, 19569–19585, <https://doi.org/10.1029/1999JD900232>, 1999.
- 785 Koren, V., Smith, M., and Cui, Z.: Physically-based modifications to the Sacramento Soil Moisture Accounting model. Part A: Modeling the effects of frozen ground on the runoff generation process, *J. Hydrol.*, 519, 3475–3491, <https://doi.org/10.1016/j.jhydrol.2014.03.004>, 2014.
- Kouwen, N.: WATFLOOD/WATROUTE Hydrological Model Routing & Flow Forecasting System., Department of Civil and Water Engineering, University of Waterloo, Waterloo, Canada, 267 pp., 2010.
- 790 Krogh, S. A. and Pomeroy, J. W.: Simulating site-scale permafrost hydrology: Sensitivity to modelling decisions and air temperature, *J. Hydrol.*, 602, 126771, <https://doi.org/10.1016/j.jhydrol.2021.126771>, 2021.
- Krogh, S. A., Pomeroy, J. W., and Marsh, P.: Diagnosis of the hydrology of a small Arctic basin at the tundra-taiga transition using a physically based hydrological model, *J. Hydrol.*, 550, 685–703, <https://doi.org/10.1016/j.jhydrol.2017.05.042>, 2017.
- 795 Kurylyk, B. L. and Watanabe, K.: The mathematical representation of freezing and thawing processes in variably-saturated, non-deformable soils, *Adv. Water Resour.*, 60, 160–177, <https://doi.org/10.1016/j.advwatres.2013.07.016>, 2013.
- Lampe, D. C.: Hydrogeologic Framework of Bedrock Units and Initial Salinity Distribution for a Simulation of Groundwater Flow for the Lake Michigan Basin, U.S. Geological Survey, Reston, Virginia, 58 pp., 2009.
- Larsbo, M., Roulier, S., Stenemo, F., Kasteel, R., and Jarvis, N.: An Improved Dual-Permeability Model of Water Flow and Solute Transport in the Vadose Zone, *Vadose Zone J.*, 4, 398–406, <https://doi.org/10.2136/vzj2004.0137>, 2005.
- 800



- Leonardini, G., Anctil, F., Abrahamowicz, M., Gaborit, É., Vionnet, V., Nadeau, D. F., and Fortin, V.: Evaluation of the Soil, Vegetation, and Snow (SVS) Land Surface Model for the Simulation of Surface Energy Fluxes and Soil Moisture under Snow-Free Conditions, *Atmosphere*, 11, 278, <https://doi.org/10.3390/atmos11030278>, 2020.
- Leonardini, G., Anctil, F., Vionnet, V., Abrahamowicz, M., Nadeau, D. F., and Fortin, V.: Evaluation of the snow cover in the
805 Soil, Vegetation, and Snow (SVS) land surface model, *J. Hydrometeorol.*, <https://doi.org/10.1175/JHM-D-20-0249.1>, 2021.
- Lindström, G., Bishop, K., and Löfvenius, M. O.: Soil frost and runoff at Svartberget, northern Sweden—measurements and model analysis, *Hydrol. Processes*, 16, 3379–3392, <https://doi.org/10.1002/hyp.1106>, 2002.
- Liu, Y., Wang, X., Wen, Y., Cai, H., Song, X., and Zhang, Z.: Effects of freeze-thaw cycles on soil greenhouse gas emissions: A systematic review, *Environ. Res.*, 248, 118386, <https://doi.org/10.1016/j.envres.2024.118386>, 2024.
- 810 Lundin, L.-C.: Hydraulic Properties in an Operational Model of Frozen Soil, *J. Hydrol.*, 118, 289–310, [https://doi.org/10.1016/0022-1694\(90\)90264-X](https://doi.org/10.1016/0022-1694(90)90264-X), 1990.
- Mao, L., Wang, C.-Y., and Tabuchi, Y.: A Multiphase Model for Cold Start of Polymer Electrolyte Fuel Cells, *J. Electrochem. Soc.*, 154, B341, <https://doi.org/10.1149/1.2430651>, 2007.
- McTaggart-Cowan, R., Vaillancourt, P. A., Zadra, A., Chamberland, S., Charron, M., Corvec, S., Milbrandt, J. A., Paquin-
815 Ricard, D., Patoine, A., Roch, M., Separovic, L., and Yang, J.: Modernization of Atmospheric Physics Parameterization in Canadian NWP, *J. Adv. Model. Earth Syst.*, 11, 3593–3635, <https://doi.org/10.1029/2019MS001781>, 2019.
- Miller, R. D.: Scaling of Freezing Phenomena in Soils, in: *Applications of Soil Physics*: edited by: Hillel D., Elsevier, Amsterdam, Netherlands, 254–299, <https://doi.org/10.1016/B978-0-12-348580-9.50016-X>, 1980.
- Mohammed, A. A., Cey, E. E., and Hayashi, M.: Snowmelt Infiltration and Macropore Flow in Frozen Soils: Overview,
820 Knowledge Gaps, and a Conceptual Framework, *Vadose Zone J.*, 17, 1–15, <https://doi.org/10.2136/vzj2018.04.0084>, 2018.
- Mohammed, A. A., Pavlovskii, I., Cey, E. E., and Hayashi, M.: Effects of preferential flow on snowmelt partitioning and groundwater recharge in frozen soils, *Hydrol. Earth Syst. Sci.*, 23, 5017–5031, <https://doi.org/10.5194/hess-23-5017-2019>, 2019.
- Mohammed, A. A., Cey, E. E., Hayashi, M., Callaghan, M. V., Park, Y., Miller, K. L., and Frey, S. K.: Dual-permeability
825 modeling of preferential flow and snowmelt partitioning in frozen soils, *Vadose Zone J.*, 20, e20101, <https://doi.org/10.1002/vzj2.20101>, 2021.
- Mohammed, G. A., Hayashi, M., Farrow, C. R., and Takano, Y.: Improved characterization of frozen soil processes in the Versatile Soil Moisture Budget model, *Can. J. Soil. Sci.*, 93, 511–531, <https://doi.org/10.4141/cjss2012-005>, 2013.
- Nash, J. E. and Sutcliffe, J. V.: River flow forecasting through conceptual models part I — A discussion of principles, *J. Hydrol.*, 10, 282–290, [https://doi.org/10.1016/0022-1694\(70\)90255-6](https://doi.org/10.1016/0022-1694(70)90255-6), 1970.
- 830 Neri, A., Villarini, G., Slater, L. J., and Napolitano, F.: On the statistical attribution of the frequency of flood events across the U.S. Midwest, *Adv. Water Resour.*, 127, 225–236, <https://doi.org/10.1016/j.advwatres.2019.03.019>, 2019.
- Niu, G. and Yang, Z.: An observation-based formulation of snow cover fraction and its evaluation over large North American river basins, *J. Geophys. Res.: Atmos.*, 112, 2007JD008674, <https://doi.org/10.1029/2007JD008674>, 2007.



- 835 Niu, G.-Y. and Yang, Z.-L.: Effects of Frozen Soil on Snowmelt Runoff and Soil Water Storage at a Continental Scale, *J. Hydrometeorol.*, 7, 937–952, <https://doi.org/10.1175/JHM538.1>, 2006.
- NOAA: 2021 annual climate trends and impacts summary for the Great Lakes Basin, NOAA, Ann Arbor, Michigan, USA, 2021.
- Patel, K. F., Tatariw, C., MacRae, J. D., Ohno, T., Nelson, S. J., and Fernandez, I. J.: Soil carbon and nitrogen responses to snow removal and concrete frost in a northern coniferous forest, *Can. J. Soil. Sci.*, 98, 436–447, <https://doi.org/10.1139/cjss-2017-0132>, 2018.
- 840 Penfound, E. and Vaz, E.: Analysis of 200 years of change in ontario wetland systems, *Appl. Geogr.*, 138, 102625, <https://doi.org/10.1016/j.apgeog.2021.102625>, 2022.
- Perry, C. A.: Significant Floods in the United States During the 20th Century - USGS Measures a Century of Floods, U.S. Geological Survey, Reston, Virginia, 3 pp., 2000.
- 845 Pitman, A. J., Yang, Z.-L., Cogley, G., and Henderson-Sellers, A.: Description of bare essentials of surface transfer for the Bureau of Meteorology Research Centre AGCM, School of Earth Sciences, Macquarie University, Melbourne, Australia, 117 pp., 1991.
- Ross, P. J. and Smettem, K. R. J.: A Simple Treatment of Physical Nonequilibrium Water Flow in Soils, *Soil Sci. Soc. Am. J.*, 850 64, 1926–1930, <https://doi.org/10.2136/sssaj2000.6461926x>, 2000.
- Shanley, J. B. and Chalmers, A.: The effect of frozen soil on snowmelt runoff at Sleepers River, Vermont, *Hydrol. Processes*, 13, 1843–1857, [https://doi.org/10.1002/\(SICI\)1099-1085\(199909\)13:12/13<1843::AID-HYP879>3.0.CO;2-G](https://doi.org/10.1002/(SICI)1099-1085(199909)13:12/13<1843::AID-HYP879>3.0.CO;2-G), 1999.
- Šimůnek, J., Jarvis, N. J., Van Genuchten, M. Th., and Gärdenäs, A.: Review and comparison of models for describing non-equilibrium and preferential flow and transport in the vadose zone, *J. Hydrol.*, 272, 14–35, [https://doi.org/10.1016/S0022-1694\(02\)00252-4](https://doi.org/10.1016/S0022-1694(02)00252-4), 2003.
- 855 Six, J., Bossuyt, H., Degryze, S., and Deneff, K.: A history of research on the link between (micro)aggregates, soil biota, and soil organic matter dynamics, *Soil Tillage Res.*, 79, 7–31, <https://doi.org/10.1016/j.still.2004.03.008>, 2004.
- Smirnova, T. G., Brown, J. M., Benjamin, S. G., and Kim, D.: Parameterization of cold-season processes in the MAPS land-surface scheme, *J. Geophys. Res.*, 105, 4077–4086, <https://doi.org/10.1029/1999JD901047>, 2000.
- 860 Soulis, E. D., Snelgrove, K. R., Kouwen, N., Seglenieks, F., and Verseghy, D. L.: Towards closing the vertical water balance in Canadian atmospheric models: Coupling of the land surface scheme class with the distributed hydrological model watflood, *Atmos. Ocean*, 38, 251–269, <https://doi.org/10.1080/07055900.2000.9649648>, 2000.
- Stähli, M.: Hydrological significance of soil frost for pre-alpine areas, *J. Hydrol.*, 546, 90–102, <https://doi.org/10.1016/j.jhydrol.2016.12.032>, 2017.
- 865 Stähli, M., Jansson, P.-E., and Lundin, L.-C.: Preferential Water Flow in a Frozen Soil - A Two-Domain Model Approach, *Hydrol. Processes*, 10, 1305–1316, [https://doi.org/10.1002/\(SICI\)1099-1085\(199610\)10:10<1305::AID-HYP462>3.0.CO;2-F](https://doi.org/10.1002/(SICI)1099-1085(199610)10:10<1305::AID-HYP462>3.0.CO;2-F), 1996.



- Stähli, M., Jansson, P., and Lundin, L.: Soil moisture redistribution and infiltration in frozen sandy soils, *Water Resour. Res.*, 35, 95–103, <https://doi.org/10.1029/1998WR900045>, 1999.
- 870 Stenemo, F. and Jarvis, N.: Users guide to MACRO 5.2, a model of water flow and solute transport in macroporous soil, Swedish University of Agricultural Sciences, Stockholm, Sweden. 47 pp., 2010.
- Swenson, S. C., Lawrence, D. M., and Lee, H.: Improved simulation of the terrestrial hydrological cycle in permafrost regions by the Community Land Model, *J. Adv. Model. Earth Syst.*, 4, 2012MS000165, <https://doi.org/10.1029/2012MS000165>, 2012.
- Taylor, G. S. and Luthin, J. N.: A model for coupled heat and moisture transfer during soil freezing, *Can. Geotech. J.*, 15, 548–
- 875 555, <https://doi.org/10.1139/t78-058>, 1978.
- Verseghy, D.: The Canadian Land Surface Scheme Technical Documentation - Version 3.4, Climate Research Division of Environment Canada, Toronto, Canada, 178 pp., 2008.
- Vionnet, V., Fortin, V., Gaborit, E., Roy, G., Abrahamowicz, M., Gasset, N., and Pomeroy, J. W.: Assessing the factors governing the ability to predict late-spring flooding in cold-region mountain basins, *Hydrol. Earth Syst. Sci.*, 24, 2141–2165, 880 <https://doi.org/10.5194/hess-24-2141-2020>, 2020.
- Vionnet, V., Leroux, N. R., Fortin, V., Abrahamowicz, M., Woolley, G., Mazzotti, G., Gaillard, M., Lafaysse, M., Royer, A., Domine, F., Gauthier, N., Rutter, N., Derksen, C., and Bélair, S.: Enhancing simulations of snowpack properties in land surface models with the Soil, Vegetation and Snow scheme v2.0 (SVS2), *Geosci. Model Dev.*, 18, 9119–9147, <https://doi.org/10.5194/gmd-18-9119-2025>, 2025.
- 885 Wang, J., Zhang, J., Xie, D., Ma, J., Zhao, Y., Ning, S., Song, C., Zhang, Z., Zhu, J., He, J.-S., and Wang, H.: Shifts in soil freeze-thaw cycle and their climate impacts along the alpine wetland-grassland continuum, *Agric. For. Meteorol.*, 367, 110506, <https://doi.org/10.1016/j.agrformet.2025.110506>, 2025.
- Wang, Y., Broxton, P., Fang, Y., Behrangi, A., Barlage, M., Zeng, X., and Niu, G.: A Wet-Bulb Temperature-Based Rain-Snow Partitioning Scheme Improves Snowpack Prediction Over the Drier Western United States, *Geophys. Res. Lett.*, 46, 890 13825–13835, <https://doi.org/10.1029/2019GL085722>, 2019.
- Watanabe, K.: Water and heat flow in a directionnaly frozen silty soil, in: Proceedings of the Third Hydrus Workshops, Prague, Czech Republic, 26-27 March 2008, 15–22, 2008.
- Wei, X., Huang, C., Wei, N., Zhao, H., He, Y., and Wu, X.: The impact of freeze–thaw cycles and soil moisture content at freezing on runoff and soil loss, *Land Degrad. Dev.*, 30, 515–523, <https://doi.org/10.1002/ldr.3243>, 2019.
- 895 Weigert, A. and Schmidt, J.: Water transport under winter conditions, *CATENA*, 64, 193–208, <https://doi.org/10.1016/j.catena.2005.08.009>, 2005.
- Yassin, F., Razavi, S., Elshamy, M., Davison, B., Sapriza-Azuri, G., and Wheeler, H.: Representation and improved parameterization of reservoir operation in hydrological and land-surface models, *Hydrol. Earth Syst. Sci.*, 23, 3735–3764, <https://doi.org/10.5194/hess-23-3735-2019>, 2019.
- 900 Zhang, L., Yang, C., Wang, D., Zhang, P., and Zhang, Y.: Freezing point depression of soil water depending on its non-uniform nature in pore water pressure, *Geoderma*, 412, 115724, <https://doi.org/10.1016/j.geoderma.2022.115724>, 2022.



- Zhang, T., Barry, R.G., Knowles K., Ling, F., and Armstrong, R.L.: Distribution of seasonally and perennially frozen ground in the Northern Hemisphere, in: Proceedings of the Eighth International Conference on Permafrost, Zurich, Switzerland, 21-25 July 2003, 2003.
- 905 Zhang, Y., Cao, Z., Hou, F., and Cheng, J.: Characterizing Preferential Flow Paths in Texturally Similar Soils under Different Land Uses by Combining Drainage and Dye-Staining Methods, *Water*, 13, 219, <https://doi.org/10.3390/w13020219>, 2021.
- Zhao, L. and Gray, D. M.: Numerical analysis of simultaneous heat and mass transfer during infiltration into frozen ground, *J. Hydrol.*, 200, 345–363, [https://doi.org/10.1016/S0022-1694\(97\)00028-0](https://doi.org/10.1016/S0022-1694(97)00028-0), 1997.